Geomorphology

Late Quaternary uplift and sea level fluctuations along the Tyrrhenian margin of Basilicata - northern Calabria (southern Italy): New constraints from raised paleoshorelines

--Manuscript Draft--

Manuscript Number:	GEOMOR-10699R1
Article Type:	Research Paper
Keywords:	Marine terraces; coastal uplift; Late Quaternary; Mediterranean Sea
Corresponding Author:	Alessandra Ascione, Ph.D. Università di Napoli Federico II Naples, ITALY
First Author:	Ciro Cerrone
Order of Authors:	Ciro Cerrone
	Alessandra Ascione, Ph.D.
	Gaetano Robustelli, PhD
	Paola Tuccimei, PhD
	Michele Soligo, PhD
	Giuseppina Balassone, PhD
	Angela Mormone, PhD
Abstract:	New analyses of marine terraces in the Tyrrhenian Sea margin of Basilicata - northern Calabria (southern Italy) have been carried out. In the study area, c. 25 km in length, an impressive flight of marine terraces occurs, with the highest terraces reaching ~160 m a.s.l. Detailed geomorphological-stratigraphical analyses on remnants of paleoshorelines located within 60 m a.s.l. have shown that the rocky coast of the investigated coastal stretch has been affected by multiple relative sea level fluctuations, during which reworking of older shorelines has occurred. Dating of coral Cladocora caespitosa and speleothems, either predating or postdating single paleoshorelines, has allowed the construction of a chronological framework for the identified relative sea-level markers, and their correlation with MIS 7, MIS 6e and distinct peaks of MIS 5. A mean uplift rate since the Last Interglacial has been evaluated in c. 0.25 mm/y, one order of magnitude larger than former estimates. The uplift rate value has been used to infer the elevations of MIS 5a, 5c and 6e peaks, which are higher than those reported in most sea-level curves worldwide and however consistent with several findings from the western Mediterranean. Our results demonstrate that a mere sequential correlation may be misleading in the interpretation of flights of marine terraces, and indicates that multiple age controls are crucial to unravelling the complex interaction between uplift and sea level fluctuations in uplifted coastal areas. The reconstructed MIS 5a, 5c and 6e paleo-elevations, besides contributing to the assessment of late Quaternary sea level fluctuations in the Mediterranean Sea basin, may contribute to constrain coeval ice sheets volume variations.

HIGHLIGHTS

- Sea-level markers in the Tyrrhenian Sea margin of southern Italy are analysed
- Morpho-stratigraphy is integrated by U-series dating of corals and speleothems
- Paleoshorelines of MIS 7, MIS 6e and the three peaks of MIS 5 are identified
- A mean uplift rate of c. 0.25 mm/y since the Last Interglacial is estimated
- The relative sea level for the peaks of MIS 5a, 5c and 6e are inferred

Abstract

New analyses of marine terraces in the Tyrrhenian Sea margin of Basilicata - northern Calabria (southern Italy) have been carried out. In the study area, c. 25 km in length, an impressive flight of marine terraces occurs, with the highest terraces reaching ~160 m a.s.l. Detailed geomorphological-stratigraphical analyses on remnants of paleoshorelines located within 60 m a.s.l. have shown that the rocky coast of the investigated coastal stretch has been affected by multiple relative sea level fluctuations, during which reworking of older shorelines has occurred. Dating of coral *Cladocora caespitosa* and speleothems, either predating or postdating single paleoshorelines, has allowed the construction of a chronological framework for the identified relative sea-level markers, and their correlation with MIS 7, MIS 6e and distinct peaks of MIS 5. A mean uplift rate since the Last Interglacial has been evaluated in c. 0.25 mm/y, one order of magnitude larger than former estimates. The uplift rate value has been used to infer the elevations of MIS 5a, 5c and 6e peaks, which are higher than those reported in most sea-level curves worldwide and however consistent with several findings from the western Mediterranean. Our results demonstrate that a mere sequential correlation may be misleading in the interpretation of flights of marine terraces, and indicates that multiple age controls are crucial to unravelling the complex interaction between uplift and sea level fluctuations in uplifted coastal areas. The reconstructed MIS 5a, 5c and 6e paleo-elevations, besides contributing to the assessment of late Quaternary sea level fluctuations in the Mediterranean Sea basin, may contribute to constrain coeval ice sheets volume variations.

Title: Late Quaternary uplift and sea level fluctuations along the Tyrrhenian margin of Basilicata - northern Calabria (southern Italy): New constraints from raised paleoshorelines

Ciro Cerrone, ciro.cerrone@unina.it
Department of Earth, Environmental and Resources Science - DiSTAR, University of Naples Federico II, Complesso Universitario di Monte Sant'Angelo, via Cinthia 21 80126, Naples, Italy.

Alessandra Ascione, corresponding author, ascione@unina.it, alessandra.ascione@unina.it
Department of Earth, Environmental and Resources Science - DiSTAR, University of Naples Federico II, Complesso Universitario di Monte Sant'Angelo, via Cinthia 21 80126, Naples, Italy.

Gaetano Robustelli, gaetano.robustelli@unical.it
Department of Biology, Ecology and Earth Science - DiBEST, University of Calabria, via P. Bucci, Cube 15b, 87036 Rende (CS), Italy.

Paola Tuccimei, paola.tuccimei@uniroma3.it
Department of Science, Roma Tre University, Largo San Leonardo Murialdo 1, 00146 Rome, Italy.

Michele Soligo, michele.soligo@uniroma3.it
Department of Science, Roma Tre University, Largo San Leonardo Murialdo 1, 00146 Rome, Italy.

Giuseppina Balassone, giuseppina.balassone@unina.it
Department of Earth, Environmental and Resources Science - DiSTAR, University of Naples Federico II, Complesso Universitario di Monte Sant'Angelo, via Cinthia 21 80126, Naples, Italy.

Angela Mormone, angela.mormone@ingv.it
Istituto Nazionale di Geofisica e Vulcanologia, Osservatorio Vesuviano, via Diocleziano 238, 80124, Naples, Italy.

Late Quaternary uplift and sea level fluctuations along the Tyrrhenian margin of Basilicata - northern Calabria (southern Italy): New constraints from raised paleoshorelines

Ciro Cerrone[1], Alessandra Ascione[1], Gaetano Robustelli[2], Paola Tuccimei[3], Michele Soligo[3], Giuseppina Balassone[1], Angela Mormone[4]

[1]Department of Earth, Environmental and Resources Science, University of Naples Federico II, Complesso Universitario di Monte Sant'Angelo, 80126, Naples, Italy.

[2]Department of Biology, Ecology and Earth Science, University of Calabria, Via P. Bucci, Cube 15b, 87036 Rende (CS), Italy.

[3]Department of Science, Roma Tre University, Largo San Leonardo Murialdo 1, 00146 Rome, Italy

[4]Istituto Nazionale di Geofisica e Vulcanologia, Osservatorio Vesuviano, Via Diocleziano 238, 80124 Naples, Italy

Abstract

New analyses of marine terraces in the Tyrrhenian Sea margin of Basilicata - northern Calabria (southern Italy) have been carried out. In the study area, c. 25 km in length, an impressive flight of marine terraces occurs, with the highest terraces reaching ~160 m a.s.l. Detailed geomorphological-stratigraphical analyses on remnants of paleoshorelines located within 60 m a.s.l. have shown that the rocky coast of the investigated coastal stretch has been affected by multiple relative sea level fluctuations, during which reworking of older shorelines has occurred. Dating of coral *Cladocora caespitosa* and speleothems, either predating or postdating single paleoshorelines, has allowed the construction of a chronological framework for the identified relative sea-level markers, and their correlation with MIS 7, MIS 6e and distinct peaks of MIS 5. A mean uplift rate since the Last Interglacial has been evaluated in c. 0.25 mm/y, one order of magnitude larger than former estimates. The uplift rate value has been used to infer the

elevations of MIS 5a, 5c and 6e peaks, which are higher than those reported in most sea-level curves worldwide and however consistent with several findings from the western Mediterranean. Our results demonstrate that a mere sequential correlation may be misleading in the interpretation of flights of marine terraces, and indicates that multiple age controls are crucial to unravelling the complex interaction between uplift and sea level fluctuations in uplifted coastal areas. The reconstructed MIS 5a, 5c and 6e paleo-elevations, besides contributing to the assessment of late Quaternary sea level fluctuations in the Mediterranean Sea basin, may contribute to constrain coeval ice sheets volume variations.

Key words*: marine terraces, morpho-stratigraphy, geochronological dating, MIS 5, MIS 6e, Tyrrhenian margin.*

1. Introduction

In the last decades, increasing attention has been devoted to the reconstruction of sea level fluctuations recorded during interglacial periods, when warmer temperatures and depletion of ice sheets as a response of long-term orbital control triggered rises of the sea level (e.g., Imbrie et al., 1984; Shackleton et al., 1990; Lisieki and Raymo, 2005; Siddall et al., 2007, and references therein; Huybers and Aharonson, 2010). Such attention rests on the acknowledgement of the crucial importance of paleoclimatic indicators in understanding the mechanisms governing temperature change and its effects, as such issues may spread light on the present warm period and the future (e.g., Kattsov et al., 2005; Turney and Jones, 2010; IPCC, 2013). For instance, the Last Interglacial period, or Marine Isotope Stage - MIS 5e, is acknowledged as an analogous for better understanding the consequences of modern global warming (e.g., IPCC, 2013). In this

regard, paleoshorelines represent first order indicators of sea level fluctuations. In coastal sectors not affected by crustal displacements, these markers allow the reconstruction of sea level curves, which provide measures of total volume of the oceans that depends on the global glacial volume (Mörner, 1982). In fact, once the glacio-hydro-isostatic contributions, which cause the spatial variability to the field-estimated sea level worldwide, are evaluated, eustatic, or ice-volume equivalent sea level change may be determined (Lambeck and Chappell, 2001; Creveling et al., 2015). Where tectonically-induced crustal displacements occur, relative sea level (RSL) change can be reconstructed assuming a constant and known uplift rate in the studied sector (e.g., Chappell and Shackleton, 1986; Pirazzoli, 1996; Pedoja et al., 2014 and references therein; Robertson et al., 2019). Crucial to any of such reconstructions is the availability of reliable constraints to both elevation and age, such as those obtained from fossil corals, of sea level markers (e.g. Bloom et al., 1974; Bender et al., 1979; Bard et al., 1990; Chappell et al., 1996; Zazo et al., 2002; Rovere et al., 2016a).

To date a well-constrained field-based sea level change determination, essentially supported by coral dating, is available for the last interglacial-glacial cycle (e.g., Bender et al., 1979; Bard et al., 1990; Chappell et al., 1996; Stirling et al., 1998; Yokoyama et al., 2000). Furthermore, database of the RSL indicators of MIS 5e in the World's coasts and the coasts of Italy are available (Ferranti et al., 2006; Pedoja et al., 2014) and an updated and standardized MIS 5e sea-level database for the western Mediterranean Sea has been compiled in the framework of the World Atlas of Last Interglacial Shorelines (WALIS; Cerrone et al., 2021a). Data on the Last Interglacial sea level markers supported by the computation of Glacio-hydro-Isostatic Adjustment (GIA, Lambeck and Chappell, 2001; Creveling et al., 2015) and taking into consideration local tectonics effects, have allowed estimating globally the MIS 5e eustatic sea

103 level (Dutton and Lambeck, 2012; Kopp et al., 2009). However, less constrained are sea level
104 fluctuations that occurred prior to the Last Interglacial as erosion of marine terraces increases
105 with age, and assumptions of long-term constancy of uplift may be unsuitable (e.g., Pirazzoli et
106 al., 1993).
107 A region suited to the study of sea level markers and the reconstruction of sea level fluctuations
108 is the Basilicata - northern Calabria sector of the southern Tyrrhenian margin (Fig. 1a and b),
109 where coral-bearing paleoshorelines occur. Impressive flights of marine terraces testify to long-
110 term Quaternary uplift of the margin of the southern Tyrrhenian basin in the order of several
111 hundreds of metres, although the southern segment (southern Calabria) was affected by larger
112 uplift compared with the northern segment (e.g., Damiani, 1970; Dumas et al., 1987, 2000;
113 Ascione and Romano, 1999; Filocamo et al., 2009; Bianca et al., 2011; Monaco et al., 2017;
114 Cerrone et al., 2021b). The differential uplift is better expressed by the variable elevations of the
115 markers of the Last Interglacial, which in the northern segment are located at the same elevation
116 or a few metres higher than coeval indicators from stable areas in the Tyrrhenian sea margin
117 while in southern Calabria are strongly uplifted (e.g., Bordoni and Valensise, 1999; Dumas et al.,
118 1987; Esposito et al., 2003; Ferranti et al., 2006). The northward limit of the fast uplifting sector
119 is undefined due to the lack of data in a ~100 km long coastal strip (Ferranti et al., 2006). Further
120 north, the northern Calabria to Basilicata appears as a key area for the reconstruction of a
121 comprehensive framework of recent uplift of the southern Tyrrhenian margin.
122 Using a geomorphological-stratigraphic approach, we studied the relative sea-level markers that
123 occur in a ~25 km-long coastal belt extended from Basilicata to northern Calabria. The identified
124 paleoshorelines are sculpted in carbonate bedrock and characterised by shallow marine deposits
125 composed of carbonate pebbles/conglomerates and calcarenites. In several instances the marine

126 deposits bear coral *Cladocora caespitosa,* encrusting algae and mollusks and, in some outcrops,
127 either cover or are covered by carbonate cave deposits. Field evidence, constrained by U-series
128 dating of coral samples and speleothems either predating, or postdating, the identified
129 paleoshorelines allowed the reconstruction of a chronological framework for the analysed sea
130 level markers and constraining the late Quaternary uplift of the investigated area. By overall
131 data, constraints to the late Quaternary sea level history of the Tyrrhenian Sea can be inferred.
132

133 **2. Geological framework**

134 An indented coastal perimeter featuring narrow headlands and bays characterises the steep rocky
135 coast of the investigated area, which is located in the eastern margin of the Tyrrhenian Sea basin
136 (Fig. 1a), from Maratea, in the north, to Scalea (Fig. 1b). The rocky backbone of the study area is
137 formed of Triassic to Miocene carbonates that are tectonically overlain by ophiolitic nappes
138 (Iannace et al., 2005; 2007), with both units being part of the southern Apennines fold and thrust
139 belt (Fig. 1b). Neogene to Quaternary NE-verging thrusting in the southern Apennines were
140 coeval, since the late Miocene, with back-arc extension in the Tyrrhenian Sea basin, with both
141 processes being related to the roll back of the west-dipping Apulian-Ionian slab (e.g., Malinverno
142 and Ryan, 1986; Patacca et al., 1990; Royden, 1993; Faccenna et al., 2001; Fig. 1a). Quaternary
143 extension in the southeastern Tyrrhenian basin affected the southern Apennines margin with
144 formation of a series of coastal grabens (e.g., Rehault et al., 1987; Caiazzo et al., 2006). In the
145 horst blocks, Quaternary marine terraces testify to the attainment, since the Early Pleistocene, of
146 a coastal perimeter that approximates the modern one (Ascione and Romano, 1999; Filocamo et
147 al., 2009). Ceasing of shortening in the southern Apennines at ~0.7 Ma was followed by
148 regional-scale uplift of the mountain range and foothills to the east of it occurred in response to

149 detachment and rebound of the Ionian slab (Cinque et al., 1993; Patacca and Scandone, 2001;
150 Ascione et al., 2012). Fast uplift with rates >1 mm/y is inferred from late Quaternary raised
151 marine terraces along the Ionian coastal belt and Tyrrhenian coast of southern Calabria (e.g.,
152 Dumas et al., 1987; Miyauchi et al., 1994; Bordoni and Valensise, 1999; Amato, 2000; Ferranti
153 et al., 2006; Bianca et al., 2011; Monaco et al., 2017). Consistently, geomorphic evidence from
154 the Aspromonte massif (southern Calabria) indicates slow uplift in the Early Pleistocene
155 followed by pulses of rapid uplift during the late Quaternary (Robustelli, 2019). In southern
156 Calabria, raised Holocene shorelines indicate fast uplift continuing nowadays due to the
157 summation of a regional plus a local component associated with the activity of large normal
158 faults, which would account for values ranging between 0.1 and 0.7 mm/yr of vertical fault slip
159 (e.g., Ghisetti, 1992; Westaway, 1993; Miyauchi et al., 1994; Bordoni and Valensise, 1999;
160 Tortorici et al., 2003; Ferranti et al., 2007). The rapidly uplifting region is well correlated with
161 sectors characterised by high seismic release (e.g., Antonioli et al., 2006; Ferranti et al., 2007),
162 with devastating historical earthquakes occurred in 1783, 1908 and 1925 (Rovida et al., 2021). A
163 more subdued seismicity characterises the Basilicata – northern Calabria coastal belt, where
164 inland and offshore historical seismicity is sparse and of moderate energy ($M \leq 5$; Rovida et al.,
165 2021).
166 A flight of marine terraces reaching elevations ranging from ~130 m, in the north, to ~160 m, in
167 the south (Filocamo, 2007; Filocamo et al., 2009) characterises our study area. As most marine
168 terraces are undated, there is a long debate on their chronological framework, e.g., the highest
169 marine terrace (130–160 m a.s.l.) has been correlated with MIS 5e by Westaway (1993) and
170 framed in the late Early Pleistocene by Filocamo et al. (2009). These authors correlated with
171 MIS 19 a marine terrace located 100 m a.s.l. in the San Nicola Arcella - Scalea sector (Fig. 1b)

and highlighted that block-faulting accompanying uplift substantially ceased since the Middle Pleistocene. The chronological framework by Filocamo et al. (2009) relies on literature dating on coral *Cladocora caespitosa* and D/L measurements on bivalves by Carobene et al. (1986) and Carobene and Dai Pra (1991), who correlated the marine terraces in the ~12–17 m and ~5–9 m elevation ranges with the late MISs of the Middle Pleistocene and MIS 5e, respectively, and terraces in the ~5–2 m range to either MIS 5c or MIS 5a. By these data, Ferranti et al. (2006) inferred an uplift rate in the range of 0.05–0.03 mm/y since the Last Interglacial.

3. Materials and Methods

The study was based on the combination of geomorphological-stratigraphical analyses with new geochronological analyses. As both the marine and overlying continental deposits are carbonate in nature, methods such as Optically Stimulated Luminescence - OSL dating that provides reliable ages for late Quaternary marine terraces (e.g., Ramos et al., 2012; Carvalhido et al., 2014), could not be used in our study. However, colonies of coral *Cladocora caespitosa* are widespread in the marine terraces we analysed, along with calcareous speleothems either predating or postdating the identified sea level markers. Speleothems and corals are considered excellent samples to be dated with U-series disequilibria methods because in most cases they consist of pure calcium carbonate, free from a detrital component that makes problematic the dating of dirty carbonates. Paleoshorelines dating was thus based on U-series analyses of coral samples, pre-treated through mineralogical analyses. Dating of speleothems was used to constrain the ages of marine deposits not bearing corals, or bearing undated corals due to weathering/recrystallization, or to cross-check dating of corals. Specifically, the analysed speleothems consist of flowstones, i.e. coverings of cave floor and walls that accrete roughly

parallel to the host surface (Ford and Williams, 1989). Stable isotope analyses were performed at Bochum University (Institut für Geologie, Mineralogie und Geophysik, Ruhr-Universität) to constrain the water formational environment of three speleothems. The age model we obtained for the marine terrace flight was used for estimations of the uplift rate and elevations of paleo-sea level at different late Quaternary sea level peaks.

3.1 Geomorphological-stratigraphical approach

In order to outline the coastal geomorphology framework of the study area, we first mapped the flights of terraced surfaces in the entire investigated coastal belt, with a particular focus on the terraces located in the first tens of metres (~60 m) a.s.l. For the analysis of topography, we used 1:5000 scale maps and LiDAR data released by the Italian Ministry of Environment – MATTM, with resolutions of 1×1 m and 2×2 m. The marine terrace remnants are small size (ranging from a few to few tens of m) and spatially discontinuous. In the study area, as commonly along rocky coasts, information on RSL obtained from mapping of terraces using topographic data alone may be misleading unless it is integrated by detail-scale field data. In fact, slope breccia and alluvial fan sediments commonly bury the marine terrace surfaces, thus hampering RSL estimations.

Detail-scale field surveys were carried out at several sites (Fig. 1b) aimed at the: (i) identification and mapping of sea level markers, (ii) reconstruction of the relative chronology among sea level markers identified at each site, and (iii) spatial correlation among markers located in different sites. The morpho-stratigraphical reconstructions were focused on the detection of erosional/depositional sea level indicators and investigation of the crosscut relationships between those features and continental deposits and landforms. The depositional indicators are clastic shore deposits, calcarenites and coral and algal bioconstructions, while the erosional indicators

are abrasion platforms, tidal notches, coastal caves and *L. lithophaga* hole bands. As sea-level markers, we considered the abrasion platform-sea cliff edges, or shoreline angles, which correspond to the highest elevation reached by the sea during interglacial periods (Lajoie, 1986). The platform inner edge is an essential geodetic marker (Jara-Muñoz et al., 2019, and reference therein) especially in the western Mediterranean where the tide range is limited (±0.25 m; Antonioli et al., 2015). The elevations of the platform inner edges were constrained by crossing topographic and GPS data, and/or using a laser distance meter. The positions of the inner edges, where buried by continental covers, were geometrically reconstructed using the intersection point between the profiles of the paleo-sea cliffs and marine platforms. The error in the elevation of the sea level markers ranges from some dm to 1 m depending on whether the inner edge is apparent or buried.

3.2 U-series dating and mineralogical characterization of corals

The $^{230}Th/^{234}U$ method is the most widely used dating technique applied to continental carbonate deposits and corals and is based on the extreme fractionation of the parent isotopes ^{238}U and ^{234}U from their long-lived daughter ^{230}Th in the hydrosphere (Edwards et al., 2003). On the contrary, molluscs are not suitable for U-series dating due to an open-system postmortem history, in fact the discrepancy between the U-series dating on corals and molluscs could be from ten to hundred of thousand years because of postmortem processes of U-uptake not quantitatively quantified (Kaufman et al., 1971, 1996; Ivanovich et al., 1983; Carobene et al., 1986). Uranium, markedly more soluble than Th in the surface and near-surface environments, is readily mobilised as the highly soluble uranyl ion (UO_2^{2+}) and its complexes, whereas Th is easily hydrolysed and precipitated or adsorbed on detrital particles. Uranium is co-precipitated with $CaCO_3$ on

exsolution of CO_2, while Th is generally negligible. In the absence of detrital Th, ^{230}Th only forms in situ by radioactive decay of co-precipitated U. In a closed system the extent to which the $^{230}Th/^{234}U$ activity ratio has returned towards unity is a function of time, taking into account also the state of disequilibrium between ^{234}U and ^{238}U (Kaufman and Broecker, 1965).

For corals it is important to verify their original aragonitic nature and check for the eventual presence of calcite. In fact, no-weathered corals are originally made up of aragonite. The occurrence of relevant calcite indicates that weathering processes have affected the coral after its burial, with consequent opening of the chemical system. Therefore, a mineralogical characterization of coral samples was carried out through the X-ray powder diffraction (XRD) method. Each sample of coral and speleothem has been cleaned mechanically by washing it with de-ionized water and ultrasonically cleaned for a few minutes. Then, the preparation of coral samples consists in dividing the corals between the internal septas from their external walls with the help of a microdriller because the different thickness may react differently to the weathering processes (Roberts et al., 2009). Hence, most samples were split in two sub-samples, distinguished by labels w (wall) and s (septas).

For routine mineralogical characterization of coral samples a GE-Seifert MZVI automated diffractometer (XRD) was used, with CuKα radiation, 40 kV and 30 mA, 5s per step and a step scan of 0.05° 2θ in the 3–70° 2θ interval. The software package RayfleX (GE Inspection Technologies, 2004) was used for data processing, and phase identification was made by means of the ICDD-PDF2 database. For quantitative XRD phase analysis, i.e. calculation of percentages of aragonite, calcite and all the other associated minerals, we used both the GE-Seifert MZVI instrument (counting 18s per step, step scan 0.02° 2θ) and a PANalytical diffractometer,

263 equipped with a high speed PIXcel detector, Ni-filtered, CuKα radiation, pyrolytic graphite
264 crystal monochromator, 40 kV and 40 mA, step size of 0.02° and scanning time 8 s/step. The
265 data were refined using the Rietveld method (Bish and Post, 1993, and references therein); the
266 XRD spectra were elaborated with multiple refinements by the GSAS package (General
267 Structure Analysis System; Larson and Von Dreele, 2004) and its graphical interface EXPGUI
268 (Toby, 2001), as well as with HighScore Plus software. The Rietveld structural models were
269 based on the American Mineralogical Crystal Structure Database (AMCSD, Downs et al., 2003).
270 For U-series analyses only *Cladocora caespitosa* corals with > 95% aragonite have been used.
271 About 3 g of corals and 40 g of calcite from speleothems were selected and dissolved in nitric
272 acid. Few millilitres of hydrogen peroxide were added and heated at 100 °C in order to destroy
273 organic matter. Isotopic complexes of uranium and thorium were extracted according to the
274 procedure described in Lawrence Edwards et al. (1987) and alpha-counted using high-resolution
275 ion implanted Ortec silicon surface barrier detectors. The ages were calculated by means of
276 Isoplot/Ex (version 3.0), a plotting and regression program designed by Ludwig (2003) for
277 radiogenic-isotope data.
278
279 *3.3 Estimations of uplift and paleo-sea levels*
280 Paleoshoreline dating allowed identification of the Last Interglacial sea level markers. Using as a
281 reference the MIS 5e sea level marker, we evaluated the uplift rate by applying the classical
282 Lajoie (1986) equation [1]:
283 [1] $U=(E-pSL)/T$
284 where U is the uplift rate, E is the elevation of MIS 5e sea-level marker (in our instance, the
285 inner edge), T is the approximate time of platform bevelling (Gardner et al., 2001; Rovere et al.,

2016a) and pSL is the elevation of the paleo-sea level at time T. The error (εU) associated with the obtained uplift rate value was calculated using the error propagation formula by Morel et al. (2021), which computes the error associated with both depositional and erosional sea level markers, modified according to our case study (i.e., considering the platform inner edge as the sea level marker) as follows [2]:

[2] $$\varepsilon U = (E - pSL) \times \sqrt{(\varepsilon T/T)^2 + (\sqrt{(\varepsilon pSL^2 + \varepsilon Li^2 + \varepsilon Fm^2)/E})^2}$$

where: εT indicates MIS 5e age range; εpSL is the error in MIS 5e paleo-sea level elevation; εLi is the error in the LiDAR dataset; εFm is the error in field measurements.

The uplift rate value was assumed as constant and used to infer, from Eq. [1], paleoelevations of distinct sea level peaks both younger and older than MIS 5e. The error εpSLn associated with the determination of a paleo-sea level peak n was, then, calculated by equation [3]:

[3] $$\varepsilon pSL = pSL_n \times \sqrt{(\varepsilon U/U)^2 + (\varepsilon T_n/\ T_n)^2 + \left(\sqrt{(\varepsilon {Li_n}^2 + \varepsilon {Li_n}^2)/pSL_n}\right)^2}$$

4. Geomorphological-stratigraphical features of the marine terraces

The rocky coast extended from Basilicata to northern Calabria is characterised by narrow coastal plains and indented promontories (Fig. 2). The largest coastal plain occurs between the Castrocucco headland and Dino Island, while narrower coastal plains occur between the Torre Fiuzzi and Grotta del Prete headlands and in the Fiumicello bay (Fig. 2). The rocky slopes of headlands and cliffs behind the coastal plains are mainly composed of densely fractured dolostones or dolomitic limestones (Iannace et al., 2007; Fig. 1b), onto which marine terraces are sculpted. Large and thick alluvial fans and slope breccia sourced by the fractured carbonate bedrock almost systematically hide the terrace inner edges (Fig. 2).

The remnants of the highest terrace form a rather continuous belt of wide surfaces that progressively rise southwards, from 130 m to 160 m a.s.l., while the lower marine terraces are much smaller (Fig. 2). The abrasion terraces are frequently marked by *L. lithophaga* holes and typically mantled by patches of conglomerates and arenites of carbonate nature, sometimes rich in bivalves, e.g. *Spondylus*, *Ostrea* and *Cerastoderma*. Algal and coral (*Cladocora caespitosa*) bioconstructions are widespread in the marine terraces located up to c. 40 m a.s.l. These terraces, and those located up to c. 60 m a.s.l., are the main focus of our study. In the investigated coastal belt, evidence of reshaping of both subaerial landscape by coastal processes, and marine landforms by subaerial processes, testify to a multistage geomorphic evolution. Based on overall data, we distinguished five paleoshorelines labelled T1 to T5 (Fig. 2). In the following sections, morpho-stratigraphical characterisations of some key outcrops of the various paleoshorelines are provided, along with reconstructions of the relative chronology of the coastal and subaerial sculpturing events. The outcrops described below are the most explanatory for the reconstruction of the relative sea-level history, due to the presence of multiple geomorphological/stratigraphical evidences constrained by geochronological data.

4.1 Paleoshoreline T1

The lowest marine terrace crops out extensively in the northern part of the investigated coastal belt (e.g., Fiumicello, Ogliastro, Marina di Maratea, Maratea port sites) and in the Torre Talao sea stack, which rises above the beach of Scalea (Fig. 2 and 2a). The best exposures of marine terrace T1 occur in the northern flank of the Fiumicello bay and adjacent Ogliastro Cape (Fig. 3). Because of a continental cover the terrace inner edge is not exposed in those sites, and its outcropping innermost part is located 5 m a.s.l. (Fig. 3a).

331 The Fiumicello terrace is marked by marine deposits (hereinafter, T1 deposit) mostly composed
332 of calcarenites bearing bivalves and both fragments and globular colonies of *C. caespitosa* corals
333 (samples FMC01, FMCO8 and OGL3; Fig. 3b). At the northern border of the Fiumicello bay,
334 conglomerate lenses made up of well-rounded pebble to cobble-sized carbonate clasts are
335 interspersed within the calcarenite. The T1 deposit rests erosively on calcareous bedrock and is
336 covered by tens of m of alluvial fan deposits (hereinafter, UU; Fig. 3) consisting chiefly of
337 bedsets of massive to crudely stratified, locally amalgamated, pebble-to-cobble conglomerates;
338 basal bedding contacts are sharp and irregular, with relief of up to 0.7 m.
339 The Ogliastro terrace (Fig. 2a and 3e) is eroded on beachface deposits (hereinafter, OG deposit)
340 resting erosively on calcareous bedrock. The OG deposit consists of well-stratified sand and
341 gravel beds that are typically well-sorted and well segregated into horizontal to gently inclined
342 seaward beds with inclination of up to 5° (Fig. 3f). Beds show distinct vertical variations in clast
343 sorting size, ranging from sand to fine pebble, and are occasionally composed of bimodally
344 sorted, rounded pebbles. Seaward the beds tend to wedge out forming low-angle cross-stratified
345 bundles. The OG deposit is dissected by sub-vertical, roughly N-S trending fractures and
346 crevices filled with the foregoing T1 calcarenite (Fig. 3f). The marine succession is capped by
347 UU deposits consisting of alternating massive to crudely stratified, locally amalgamated, pebble-
348 to-cobble sized gravel beds and clast-supported sheet conglomerates occurring in laterally
349 continuous beds that extend up to 20 m.
350 In the Fiumicello and Ogliastro sites, the base of the UU deposit is marked by a reddish paleosol
351 some decimetres thick (Fig. 3d and e). Speleothems both blanket and are interspersed in the UU
352 conglomerates and cover the T1 deposit. Two laminated flowstones have been sampled for U-
353 series dating. Of the sampled speleothems, one covers the T1 deposit in the Ogliastro site

(sample OGL2) and the other, c. 3 cm thick, is part of a cave fill that includes angular breccia with a reddish matrix, which is inset in the T1 calcarenite outcropping at Fiumicello (sample FMC07; Fig. 3c).

4.2 Marine terrace T2

In the Marina di Maratea - Punta Iudia area (Fig. 1b), crosscutting relationships among erosional and depositional marine landforms indicate a composite morphostratigraphic framework. In that area, there is evidence of three marine terraces, namely T1, T2 and T4 (Fig. 2; Fig. 4a; Fig. 5a). The T2 deposit corresponds to a some metres thick marine succession (Fig. 4b), well exposed in the Marina di Maratea bay and adjacent coastal stretch; it consists of a basal, decimetre-thick conglomerate made up of pebble- to cobble-sized clasts with coarse sand matrix, passing upward into about 4 m thick bioconstruction made up of encrusting algae, gastropods, bivalves and a large amount of colonial corals and fragments of *C. caespitosa.* Multiple evidences indicate that the T2 deposit buries a pre-existing coastal morphology sculpted in the carbonate bedrock. The buried coastal morphology consists of a planar, sub-horizontal abrasion platform and relative paleo-sea cliffs, with inner edge at +5 m (Fig. 4c), which we correlate with paleoshoreline T1. Evidences indicating that paleoshoreline T1 predates the T2 deposits are (i) lithophaga holes, locally filled by calcarenites, which are densely distributed along the carbonate paleo-sea cliffs associated with the T1 (northern side of the Marina di Maratea bay; Fig. 4d-f), and (ii) the basal conglomerate of the T2 marine succession, which regularly covers the T1 abrasion platform but is missing on top of the coastal promontories around the Marina di Maratea bay, where the T2 marine deposit consists only of a thin calcarenite cover (e.g., southern side of the Marina di Maratea bay; Fig. 5).

377 Marine terrace T2 corresponds to the eroded top surface of the carbonate bedrock suspended
378 above the paleo-sea cliffs of terrace T1. Such a surface, which is overall planar, slightly seaward
379 dipping and largely patched by calcarenites (Fig. 5c), is interpreted as an abrasion surface; it
380 ranges in elevation from 6–8 m (outer rim) to 15 m, where its inner edge is well exposed in the
381 headland to the south of the Marina di Maratea bay (Fig. 4a). Landwards, in the Marina di
382 Maratea bay southern side, the T2 surface is covered by coarse grained slope breccia (Fig. 5e),
383 while in the northern side the T2 deposit is covered by alluvial fan deposits (Fig. 5d) composed
384 of stratified, fine- to coarse-pebble conglomerates, with angular gravel clasts set in reddish silty
385 to sandy matrix. Beds are ungraded and extend laterally for metres, even though low angle
386 erosive bases occasionally occur.
387 South of Marina di Maratea, at Punta Iudia (Fig. 5a), the T2 conglomerates and calcarenites form
388 neptunian dikes filling several m deep, subvertical crevices in the carbonate bedrock. Here an
389 apparent reddish paleosol is interposed between the T2 deposit and the slope deposit cover,
390 which consists of massive to crudely stratified conglomerates made up of angular to subangular,
391 pebble- to boulder-sized clasts; basal bedding contacts are irregular and locally sharp; the matrix
392 is locally abundant and consists of a mixture of greyish and brownish poorly-sorted sand and silt.
393 *C. caespitosa* bioconstructions have been sampled both in the Marina di Maratea bay (samples
394 MMR10 and MMR11) and Punta Iudia (sample PDR) sites.
395 In the Punta Matrella - Santojanni area (Fig. 1b) well developed marine terraces that we correlate
396 with T2 are suspended above the modern sea cliffs at +8–9 m (outer rim of the abrasion
397 surfaces), from which they gently rise landwards. In the northern border of the Santojanni bay,
398 the T2 platform is marked by patches of calcarenites and coarse-grained conglomerates, which
399 include clasts potholed by lithophaga. In the Punta Matrella headland, an abrasion surface rising

up to 15 m a.s.l., where the inner edge is locally apparent, is potholed by lithophaga and patched by conglomerates and calcarenites rich in bivalve shells and balanides. Where not exposed, the innermost parts of marine terrace T2 are covered by subaerial deposits generally composed of alluvial fan sediments and, in some instances, slope breccia. Both alluvial fan and slope breccia deposits are composed of crudely stratified unconsolidated beds made up of pebble- to cobble-sized clasts set in a reddish matrix. Outcrops of this coastal stretch reveal that marine terrace T2 has been reworked by coastal processes after its formation. This reworking is inferred from the presence of arenites and fine-grained conglomerates, which rest erosively on the T2 deposit. Specifically, they patch an irregular morphology and fill crevices and potholes sculpted on the T2 deposit (Fig. 5b). Locally (on the c. +15 m platform in the inner boundary of the Marina di Maratea bay; Fig. 5c), thin remnants of continental conglomerates with reddish matrix are interposed between the arenites and the underlying, eroded T2 bioconstructions (Fig. 5e).

In the Marina di Maratea - Punta Iudia coast, the T2 deposits and carbonate bedrock are affected by metre-size horizontal caves and conduits occasionally filled with continental breccia, coated and floored by laminated flowstones (Fig. 5d). We sampled for U-series dating the laminated speleothems that floor two caves located in the Marina di Maratea bay (samples MMR2 and MMR12; Supplementary Figure S1) and a cave formed in the T2 calcarenite in the Punta Iudia site (sample PDA2).

4.2.1 Paleoshoreline T2 in the Scalea site

Marine terrace T2 is the lowest in a flight of three terraces that shape the headlands of the Scalea coast (Fig. 1b; Fig. 2e). In the sea cliffs just to the north of the Scalea village (Fig. 6a), the T2 terrace consists of a slightly sea-dipping abrasion platform, marked by lithophaga holes and

423 covered by patches of coarse-grained sandstones to fine-pebble-grade gravels and
424 bioconstructions, which consist of encrusting algae, bryozoans, gastropods and colonies and
425 fragments of *C. caespitosa* occasionally developing decimeter-size globular growth forms (Fig.
426 6b). The calcarenites are affected by potholes (Fig. 6c) and crevices coated by speleothems and
427 covered by slope and colluvial deposits (Fig. 6e), which indicate subaerial conditions postdating
428 the formation of T2. A *C. caespitosa* colony and a flowstone coating a coral bioconstruction
429 have been sampled for U-series dating (samples SLC and SLC05, respectively). The slope
430 deposits, several metre-thick and extensively outcropping in the sea cliff at the inner border of
431 the bay, consist of stratified, up to 20° inclined, clast-supported conglomerates made up of
432 angular to subangular, pebble- to boulder-sized clasts. The matrix is composed of reddish and
433 yellowish fine-grained sediments, and is locally abundant to form occasionally matrix-supported
434 beds (Fig. 6e).
435 At Scalea, the T2 abrasion platform is located at elevations > 12 m (outer edge). For the T2 inner
436 edge, which is hidden by the slope deposits, we inferred an elevation in the range of 16±1 m by
437 integrating GPS measurements with topographic data.
438 The Scalea T2 calcarenites are affected by lithophaga holes (Fig. 6d) filled by yellowish and
439 reddish fine-grained sediments, which represent the distal and basal part of the above mentioned
440 slope deposits. Overall, the similarity of this outcrop with terrace T2 in the Marina di Maratea -
441 Punta Iudia sites suggests that the lithophaga holes result from a marine reshaping of marine
442 terrace T2.
443
444 *4.3 Sea-level markers around 20 m a.s.l.: paleoshoreline T3*

445 At several sites along the coastal stretch between the Castrocucco and Scalea headlands, there is
446 evidence for raised sea level markers at elevations ≥ 20 m, which we label T3. The best exposure
447 in these markers is that of Grotta del Prete site (Fig. 1b; Fig. 2d) where an abrasion platform cuts
448 the limestone bedrock (Fig. 7a).
449 The inferred elevation of the platform inner edge is +22 m with a ±1 m uncertainty because of a
450 colluvial cover. The abrasion platform is mantled by an up to 20 cm thick conglomerate
451 composed of pebble- to boulder-size clasts. The matrix is locally abundant and consists of
452 coarse- to very coarse-grained sandstone. An overlying biocontruction consists of encrusting
453 algae, bryozoans, gastropod and bivalve shells, and colonial *C. caespitosa* corals (samples GRP1
454 and GRP2; Fig. 7b). The bioconstructed body is blanketed by coarse-grained sandstones to
455 granule-grade deposits showing horizontally to low-angle lamination; at the top beds are bundled
456 into weakly discordant sets (Fig. 7c). The sandstones are common as infill of bioconstruction
457 crevices and potholes as well as mantle the basal gravel lag. Evidence of pedogenesis at the top
458 of these sediments indicates a subaerial exposure (Scarciglia et al., 2006).
459 Evidence of the T3 paleoshoreline is widespread in the sea cliffs behind the Praia coastal plain
460 and to the south of the Grotta del Prete site. At Pantano site (Fig. 2) a RSL rise up to +20 m is
461 testified by a bioconstruction with encrusting algae, gastropods, bivalves and coral fragments,
462 and lithophaga holes. These are covered by a speleothem sampled for dating (sample PNT). At
463 Ginnasio site (Fig. 2) an abrasion platform cut in calcareous-dolomitic bedrock with a well-
464 exposed inner edge at 20 m crops out. The platform is potholed by lithophaga holes well
465 apparent also along some crevices, which preserve decimeter-size globular growth forms of *C.*
466 *caespitosa* and bioconstructions with gastropods and encrusting algae. The crevices are also
467 filled with massive subrounded, pebble- to cobble-sized gravels interpreted as deposited at the

base of the paleo sea-cliffs, as also suggested by the presence of occasional clasts of beach conglomerates sourced by the outer edge retreat of the terrace above. Paleoshoreline T3 may be correlated southward with both massive and ungraded conglomerates made up of subrounded, pebble- to boulder-sized clasts (locally potholed by lithophaga) that mantle the cliff behind the beach of San Nicola Arcella at about +20 m, and abrasion platforms, lacking in marine deposits, on top of an isolated rock within the beach of San Nicola Arcella (+19 m) and at Torre San Nicola (inner edge at ~20 m).

Evidence of paleoshoreline T3 occurs also in the Castrocucco headland (Fig. 2). In the southwestern part of the that headland, a marine terrace carved on carbonate bedrock in the west and on well-cemented slope deposits in the east, crops out from 15 m (outer rim) to 20 m (inner edge). The sedimentary cover consists of a basal conglomerate composed of pebble- to fine cobble-size clasts passing upward to alternating coarse-grained sandstones and fine pebble-grade gravels with horizontal bedding. Regular and parallel stratification along with good clast-size sorting are indicative of swash and backwash processes in the upper beachface. Beach deposits patch laterally the paleo-sea cliff and are covered, in the east, by slope breccia. To the south (Praia - Tortora exit of the SS 18 road), beach deposits rest erosively on calcareous bedrock at c. 20 m. To the west, densely distributed lithophaga holes up to c. +20 m occur along the sea cliff at the northern boundary of the beach (Fig. 8a). At 15–20 m a.s.l. along the sea cliff at the SE headland termination, the bedrock is affected by open fissures filled by calcarenites and coated by few cm thick laminated flowstones (Fig. 8b). One of these concretions (sample CSC8, Fig. 8d) is densely potholed by lithophaga holes filled with calcarenites (Fig. 8c-d).

4.4 Paleoshoreline T4

491 The best exposure of marine terrace T4 occurs in the Torre Fiuzzi area, where a wide wave-cut
492 platform has its outer edge at ~18 m; the inner edge has been detected at 35 m a.s.l. (Fig. 2c; Fig.
493 9). The platform, slightly seaward dipping, is mantled by a few m thick calcarenite bearing *C.*
494 *caespitosa* colonies, which have been sampled for Th/U analyses (samples TFZ1 and TFZ2).
495 An abrasion platform with inner edge at +30–35 m and marked by lithophaga holes patches of
496 pebble- to cobble-sized gravels occurs in the Torre Dino site. Speleothems inset in the gravels
497 have been sampled for U-series dating (sample TRR1).
498 Sea level indicators at ~40 m a.s.l. occur in the sites of Scalea (Fig. 6a), Marina di Maratea (Fig.
499 5) and along the Castrocucco headland. Here at +35–40 m there are remnants of a tidal notch
500 (Fig. 8a) and, to the east, an abrasion platform covered by dm-thick fine- to coarse-grained,
501 rounded pebbles. At the inner margin of Tortora coastal plain (Fig. 2) an abrasion platform (outer
502 edge at +20–30 m) patched by dm-thick, well-cemented rounded gravels extends for about 2 km.
503 The platform inner edge is covered by tens of m-thick alluvial fan deposits forming a planar
504 depositional slope; it is composed of clast supported, sheet conglomerates made up of alternating
505 beds of angular, pebble to fine cobble grade clasts and pebbly sandstones. Stratification is plane
506 parallel but internal truncation surfaces may be observed as well as yellowish and reddish
507 intervening paleosols.
508
509 *4.5 Paleoshoreline T5*
510 Evidence of paleoshoreline T5 is widespread in the inner margin of the Praia coastal plain and
511 southwards, down to Scalea. In the abandoned sea cliff behind the Praia coastal plain, a large
512 karst cave (Madonna della Grotta, MdG site; Fig. 2) is located from c. 50 to 65 m a.s.l. A marine
513 reshaping of the MdG cave is testified by poorly sorted, fine pebble- to sandy matrix-supported

514 conglomerate of pebble to boulder grade which mantle the southern edge of the cave (Fig. 10).
515 The conglomerates are interpreted as the result of progressive accumulation of cliff-collapsed
516 material that outcrops from 50 to 58 m a.s.l. Gravel sediments and carbonate bedrock are
517 affected by lithophaga holes. Using the upper limits of the lithophaga holes and conglomerates as
518 indicators, paleoshoreline T5 is constrained in the 55–60 m elevation range. The lithophaga holes
519 and conglomerates patched on the cave wall are mantled by a several cm-thick flowstone, the
520 basal part of which has been sampled for U-series analysis (sample MDN01; Fig 10).
521 The MdG paleoshoreline can be correlated with several abrasion platforms outcropping to the
522 north of that site in the Torre Nave and Castiglione headlands and Rosaneto (Fig. 2) where
523 lithophaga holes locally occur. To the south, the best exposures of paleoshoreline T5 occur in the
524 Scalea coast (abrasion platform at +60 m; Fig. 6a) and Ginnasio headland (Fig. 2); here an
525 abrasion platform at ~ +60 m is blanketed by a 2 m thick gravel beach deposit characterized by
526 thin and regular stratification with gentle dip (~3°) seawards. The marine sediments are covered
527 by alluvial fan deposits of which the fan landform is still recognizable. Fan sediments consist of
528 west-inclined, well-stratified, clast-supported conglomerates composed of alternating beds of
529 angular pebble to fine cobble grade and pebbly sandstone. The beds are stacked upon one
530 another, forming bedsets that tend to pinch-out both laterally and downward, occasionally
531 characterised by concave-up erosional surfaces. The alluvial fan deposits rest unconformably
532 also on the lower paleoshoreline T3 at Ginnasio site.
533

534 **5. Mineralogical analyses, U-series dating and stable isotope results**

535 X-ray diffractometry analysis has allowed selection of corals sampled for U-series dating. Based
536 on XRD results some of the samples with relatively high calcite content (20–30%) were

discarded, while the aragonitic nature of corals sampled in Scalea, Grotta del Prete, Torre Fiuzzi and Fiumicello sites, with moderate calcite amount that is always below 3%, has been assessed (Table 1). The acceptability of the analysis result (Supplementary Table T1) was judged by the weighted reliability factor (R_{wp}), the profile agreement factor (R_p) and a goodness of fit indicator (χ^2). In fact, on fifteen different coral samples, only four of them have been suitable for geochronological analysis, whereas all the others show a significant opening of the chemical system (Table 1).

U-series analyses, both on speleothems and corals, have shown that $^{230}Th/^{232}Th$ activity ratios are always higher than 80, indicating that samples do not contain a significant detrital fraction. Furthermore, the uranium content of corals, about 2–3 ppm, approaches the average value of uranium abundance in living corals and the initial $^{234}U/^{238}U$ activity ratio ($^{234}U/^{238}U_i$) of marine carbonates generally approaches that of the marine water. These data are an evidence of the general good quality of obtained ages. The results of the U-series analyses are summarised in Table 2.

Stable isotope analyses of the speleothems sampled at the sites of Ogliastro, Fiumicello and Torre Dino were carried out. Both calcite standards used at the Ruhr-Universität Bochum (Supplementary Table T2) were run for the calcite sequence on a ThermoFisher Scientific MAT253 equipped with a GasBench II and a ConFlo IV. The results (Supplementary Table T3 and Supplementary Figure S2) show that both $\delta^{13}C$ and $\delta^{18}O$ are negative values, which indicate that the analysed calcite samples have been deposited by freshwater solutions.

6. Discussion

The flight of marine terraces analysed with this study is characterised by distinct erosional and/or depositional sea-level markers and T1 to T4 terraces up to ~40 m of elevation are characterised

561 by *Cladocora caespitosa* bioconstructions. Based on morphostratigraphy reconstructions, we
562 have spatially correlated the terrace remnants and related them to five paleoshorelines: T1,
563 located 5+1/-0 m a.s.l.; T2, located +16±1 m; T3, with at +22±1 m; T4, in the 35–40 m range;
564 T5, in the 55–60 m range; for each paleoshoreline, the elevation range is set based on vertical
565 positions of the corresponding sea level markers (i.e., platform inner edge) along the entire
566 investigated coastal stretch. Locally, as for the Ginnasio staircase, clastic sediment exposures,
567 contact relationships between marine and continental deposits and their apparent cross-cutting
568 relationships clearly indicate that the investigated coastal stretch suffered alternating
569 morphodynamics, that is the area experienced multiple periods of marine aggradation onto which
570 slope and/or alluvial fan systems prograded. Specifically, there are sites where evidence of
571 drowning of subaerial landforms occurs, e.g. the MdG site (Section 4.4), as well as reworking by
572 coastal processes of some marine terraces during younger relative sea level rises. An example
573 occurs in the Ogliastro site, where the T1 calcarenite clearly postdates the OG marine
574 conglomerate (Section 4.1). The occurrence of N-S trending fractures that dissect the OG, a
575 feature that is not observed in any other of the analysed marine successions, is an indication of
576 the old age of the OG relative to marine terraces T1 to T5, although the paleoshoreline
577 correlative to the OG is undetermined. Particularly clear is also the reworking of paleoshoreline
578 T1 in the Marina di Maratea site (Section 4.2). It is worth noting that the best exposures of
579 paleoshoreline T1 occur in the sites of Ogliastro - Fiumicello, where the good preservation of the
580 T1 calcarenites may be related to the emplacement, probably soon after the T1 formation, of the
581 UU continental cover, which originally was much more extended seawards than at present. Such
582 interpretation is suggested by the exposure of the T1, which results from its exhumation in
583 response to differential sea cliff retreat (possibly even during the Holocene), was favoured by the

584 presence of the thin paleosol interposed between the T1 and UU deposit (Section 4.1). Absence
585 of the T1 along most of the investigated coast may result from reworking and erosion of that
586 marine terrace, where not buried and in general outside the sheltered environments, by sea
587 storms even in present times. In fact, at the terminations of several of the minor headlands, there
588 are small-size, gently inclined and low-lying (< 5 m a.s.l.) capes that could be eroded remnants
589 of the T1.
590
591 *6.1 Age model*
592 The new U-series dating on *C. caespitosa* corals differ from ages provided in previous works
593 (Carobene et al., 1986, Carobene and Dai Pra 1990, 1991). Corals, dated by U-series method in
594 these old papers, were strongly recrystallized. Calcite contents ranged between 3 and 25 %,
595 showing a significant alteration of samples after their burial. Moreover, uranium contents were
596 inversely correlated with the calcite contents, demonstrating that the process of recrystallization
597 produced a significant loss of uranium, thus opening the chemical system. Since the age is
598 directly correlated with the $^{230}Th/^{234}U$ activity ratio, a loss of uranium made higher the isotope
599 ratios, increasing the age of corals. This inference is strongly supported by the high correlation
600 coefficient ($r^2 = 0.99$) of uranium abundances of five corals versus their correspondent calcite
601 percentage (Supplementary Figure S3).
602 In addition, corals from the shoreline deposits located at higher elevation are characterised by
603 higher calcite contents and lower uranium abundances, indicating that the older the relative age
604 of corals the stronger the alteration and the consequent induced increase of the age
605 (Supplementary Figure S4). This rationale, supported by a correlation coefficient of 0.99 for 4
606 samples, suggests that the recrystallization process was constant and continuous over time.

607 Finally, the lack of correlation between the $^{234}U/^{238}U$ activity ratios and the elevation of marine
608 deposits suggests that the fluids producing the alteration were characterised by different
609 composition and the weathering processes had different intensity and duration. Based on that, the
610 coral ages are not reliable and the reconstructions based on them are to be considered misleading.
611 The new U/Th data provide a robust chronological framework for the identified paleoshorelines,
612 with ages of corals and speleothems matching those of warmer and cooler periods, respectively
613 (Table 3). All dated deposits are younger than the last warm stage of the Middle Pleistocene, i.e.
614 MIS 7, aged 190–235 ka (Waelbroeck et al., 2002).
615 In the identified paleoshorelines, the T2 is precisely dated in the Scalea site based on ages from
616 both a coral and the overlying speleothem, while coral samples from the Ogliastro, Marina di
617 Maratea and Punta Iudia deposits were unsuitable for dating due their low aragonite content
618 (Table 1). For the T1, the lag between coral and speleothems ages is too large to precisely
619 constrain the marine terrace age. The lack of multiple age controls on single paleoshorelines is,
620 however, effectively integrated by morphostratigraphic information, which allows expanding
621 spatially age constraints of the surveyed sites (Table 4).
622 The 151±11 ka old speleothem outcropping at the southeastern edge of the Castrocucco headland
623 is correlated with MIS 6 (Table 3) thus constraining the following RSL rise, proved by the
624 lithophaga holes in the speleothem, to MIS 5. Coral dating indicates that the analysed marine
625 terraces flight records each of the MIS 5 sea level peaks. The 120±7 ka coral age allows
626 correlation of paleoshoreline T4 with the Last Interglacial (Table 4), which spans from ~128 to
627 116 ka (Stirling et al., 1998; Shackleton et al., 2002) or from 130 to 118 ka according to Rohling
628 et al. (2019, and references therein). In the western Mediterranean, the Last Interglacial
629 highstand is framed between ~126 and 116 ka according to evidence from Mallorca Island

(Polyak et al., 2018), while by data from the nearby southern Cilento (Bini et al., 2020) the MIS 5e upper limit is set at 120 ka. The 98±4 ka coral age and 99±12 ka old speleothem from the Scalea site constrain paleoshoreline T2 to MIS 5c, framed between 106 and 93 ka (Lisiecki and Raymo, 2005; Spratt and Lisiecki, 2016) and further indicate correlation of the speleothem with MIS 5b (Tables 3 and 4). Correlation of paleoshoreline T2 with MIS 5c contrasts with the former attribution of the calcarenites outcropping in the Marina di Maratea site to MIS 5e based on isoleucine epimerization (Carobene and Dai Pra, 1991). Such a discrepancy may be reconciled based on recent findings from the Mediterranean area, which indicate that the high coefficients of variation for epimerization values make the distinction between substages of the same MIS difficult (Torres et al., 2013).

The 83.8±3.6 ka old coral sample from Grotta del Prete site indicates a correlation of paleoshoreline T3 with MIS 5a (Table 4), which is globally framed in the 85–80 ka range (Lisiecki and Raymo, 2005; Spratt and Lisiecki, 2016), and fits both the 84.2–82.3 ka (Tuccimei et al., 2006) and c. 82–80 ka (Dorale et al., 2010) ranges of MIS 5a estimated by data from Mallorca Island. Consistent with overall chronological framework are the ages of the speleothems that postdate paleoshorelines T2 to T4. In fact, the speleothems that postdate paleoshoreline T2 in the Marina di Maratea - Punta Iudia area correlate with MIS 5b (MMR2, 90±10 ka) and the younger MIS 4 (MMR12, 67±6 ka and PDA2, 64±6 ka; Tables 3 and 4). Similarly, correlation of paleoshoreline T3 to MIS 5a is supported by the 54.7±2.7 ka age of the speleothem that covers the lithophaga holes at c. +20 m at Pantano site, and the 78.8±7.7 ka age of the speleothem at Torre Dino is consistent with correlation of paleoshoreline T4 with MIS 5e (Tables 3 and 4).

652 The above age model results in an elevation of MIS 5a paleoshorelines higher than that of the
653 MIS 5c markers. A direct superposition between MIS 5a and MIS 5c deposits is not proven by
654 dating. However, evidence from the Scalea site of lithophaga holes affecting the T2 calcarenites,
655 and from the Marina di Maratea - Punta Iudia sites of subaerial exposure between two
656 superposed marine deposits (Sections 4.2 and 4.2.1), are both consistent with a reworking of the
657 MIS 5c marine terrace T2 during a later sea level rise. Worthy to note, the dated MIS 5a
658 bioconstruction of the Grotta del Prete terrace is mantled by arenites (Section 4.3). Clear
659 evidence of subaerial exposure at the top of the bioconstruction is not found, hence the sand
660 infills of the calcarenite crevices may result from high frequency eustatic variability over MIS
661 5a, consistent with depositional evidence of marine terraces from southernmost Calabria (Dumas
662 et al., 2005).
663 Paleoshoreline T5 is constrained by the 152+33/-26 ka age of the speleothem, which in the MdG
664 site covers the sea-level markers and can be related to MIS 6 (Tables 3 and 4). Considering the
665 karst environment that hosted the MdG paleoshoreline, it is reasonable that the marine deposits
666 patched on the cave walls were cemented soon after their deposition, fairly correlated with one of
667 the MIS 7 peaks, during the following sea level fall.
668 The coral from paleoshoreline T1 in the Fiumicello site is aged 161±18 ka, thus framed in the
669 cold MIS 6. The T1 calcarenite is postdated by two speleothems aged 78±3 ka and 82±5 ka,
670 which do not strictly constrain the T1 age. However, evidence from the Marina di Maratea site
671 indicates that the +5 m marine terrace predates the T2 deposits (Section 4.2). Further information
672 on T1 relative age can be inferred from the age vs. elevation framework for paleoshorelines T2
673 to T5 discussed above, which clearly indicates that paleoshorelines correlated with sea level
674 peaks of MIS 5 and 7 are all raised above c. +15 m. Hence, correlation of paleoshoreline T1 with

675 MIS 6e, a marked warm period recorded in the 165–175 ka time span during the cold stage MIS
676 6, is reliable (Table 4).
677 The age model discussed so far allows assessment of relative sea level positions during the late
678 Quaternary in the investigated area. The RSL curve reconstructed for the study area is shown in
679 Fig. 11. Besides elevations of the dated paleoshorelines, the curve of Fig. 11 relies on vertical
680 positions of dated speleothems, which constrain the upper limit to the elevations of coeval RSL.
681 Those constraints are supported by stable isotope results on concretions inset in the marine
682 deposits of paleoshorelines T1 (Fiumicello and Ogliastro sites) and T4 (Torre Dino site;
683 Supplementary Figure S2), which rule out a deposition from marine water that could be
684 hypothesised based only on their elevations and ages, with uncertainties on the latter ones
685 spanning on MIS 5a age (Table 3).
686
687 *6.2 Constraints to the late Quaternary uplift*
688 The new chronological framework for the analysed flight of raised marine terraces implies a
689 reappraisal of the late Quaternary uplift for the investigated area. The reconstructed RSL curve
690 represents a robust starting point for the evaluation of recent uplift. Isolating the tectonic
691 component from the curve is not straightforward, if uncertainties on eustatic elevations of late
692 Quaternary sea level peaks are considered. However, among sea level peaks that imprinted the
693 investigated coastal stretch, only on MIS 5e elevation there is a general consensus. In fact,
694 although varying worldwide as a result of GIA (e.g., Creveling et al., 2015), it is widely accepted
695 that MIS 5e sea level was higher than the present one (e.g., Waelbroeck et al., 2002; Siddall et
696 al., 2003) and set in the 2–9 m elevation range (Siddall et al., 2007; Hearty et al., 2007), with
697 +6.6 m as the most probable peak (Kopp et al., 2009). In stable areas of the Mediterranean, RSL

indicators of MIS 5e span from +2 to 8 m (Benjamin et al., 2017), being at +2–3 m in Mallorca, Balearic Islands (Vesica et al., 2000; Bardaji et al., 2009), up to +7 m in the eastern Mediterranean (Sivan et al., 2016), with a +6±3 m value considered reliable for the Mediterranean Sea (Lambeck et al., 2004) and in the range of +5–8 m in the Tyrrhenian coast of peninsular Italy (Antonioli et al., 2006, and references therein; Ferranti and Antonioli, 2007).

Using as a reference MIS 5e, we evaluated a mean uplift rate in the Last Interglacial to Present time span for our study area. The uplift rate and related error were calculated following equations [1] and [2]. For the uplift rate calculation, we used a RSL value corresponding to the mean elevation of paleoshoreline T4 (Table 4), and assumed a MIS 5e sea level value of +6 m with an error of 3 m (Lambeck et al., 2004; Antonioli et al., 2006; Ferranti and Antonioli, 2007). Then, considering that in the Mediterranean sea level peaks occur at different times according to the varying geographical location (Stocchi et al., 2018), we assumed for MIS 5e peak a 120-127 ka age range based on our coral age and data by Bini et al. (2020) from nearby areas. The resulting mean uplift rate since the Last Interglacial is of 0.255±0.021 mm/y.

The c. 0.25 mm/y uplift rate that we estimated exceeds by one order of magnitude that of 0.05–0.03 mm/y estimated by Ferranti et al. (2006) for our study area based on former dating by Carobene et al. (1986) and Carobene and Dai Pra (1990, 1991). Besides being one order of magnitude larger than coastal uplift of passive margins worldwide (e.g., Pedoja et al., 2014), the c. 0.25 mm/y value exceeds the post-Last Interglacial uplift of most of the Tyrrhenian basin margin. In fact, since the Last Interglacial most of the Tyrrhenian Sea coastal belt was substantially stable, although with some local exceptions (Bordoni and Valensise, 1999; Ferranti et al., 2006; Cerrone et al., 2021a). In contrast, fast post-Last Interglacial uplift in the range of 0.4–1.35 mm/y affected the entire southern Calabria – northeastern Sicily belt, where fault-

induced contributions are superimposed on regional scale vertical motions (e.g., Dumas et al., 1987, 2000; Bordoni and Valensise, 1999; Antonioli et al., 2006; Ferranti et al., 2006, 2007; Bianca et al., 2011; Monaco et al., 2017). Within such a framework, our study area appears as the locus of a change in the behaviour of the southern Tyrrhenian margin: it separates formerly uplifted areas that are stable at present, in the north (e.g., Sorrento peninsula and Cilento, with post-MIS 5e uplift ranging from null to 0.07 mm/y; Ferranti et al., 2006), from the fast uplifting southern Calabria. Between the latter and our study area, a c. 150 km long coastal belt occurs where marine terrace are either undated or poorly constrained and such a lack of information hampers a thoroughly reconstruction of the recent vertical motions of the southern Tyrrhenian margin. However, the raised paleoshorelines in the Basilicata – northern Calabria margin that we analysed show no net evidence of displacement both across and along the coast, and such evidence may indicate the contribution of a large-scale phenomenon governing uplift or/and faulting in the offshore, where some moderate historical earthquake is recorded (Rovida et al., 2021). Multiple indicators, e.g., raised fluvial/alluvial plain terraced deposits (Filocamo, 2009; Filocamo et al., 2009), features of topography and rivers' long profiles (Mazzoli et al., 2014; Buscher et al., 2017) and the occurrence of a long wavelength topographic bulge in northern-central Calabria (Faccenna et al., 2011), point to surface uplift involving the area spanning from the coast to the mountain belt interiors in the Basilicata – northern Calabria sector. Surface uplift appears as the response to crustal extension and associated development of high-angle normal faults (Mazzoli et al., 2014), possibly combined with large-scale, deep-seated mechanisms such as slab rebound following break off (Cinque et al., 1993; Westaway, 1993; Wortel and Spakman, 2000), or upper mantle upwelling around the edges of the non-detached part of the Ionian slab

743 located beneath southernmost Calabria (e.g., Gvirtzman and Nur, 1999; Piromallo and Morelli,
744 2003; Faccenna et al., 2011).
745
746 6.3 *Inferences on the late Quaternary sea level history*
747 With the assumption of a constant uplift of 0.255±0.021 mm/y, the fragments of the RSL curve
748 of Fig. 11 can be corrected for the tectonic component (Fig. 12).
749 Based on elevations of paleoshorelines T1 to T3 and T5, we inferred the paleoelevations of the
750 corresponding sea level peaks and calculated the correlative errors using equation [3]. The
751 inferred paleoelevations of MIS 5a and 5c peaks relative to the present mean sea level are
752 +1.35±1.01 m and -9.50±1.37 m, respectively. Global scale estimations of MIS 5a peak vary
753 between -30 m (Papua New Guinea; Lambeck and Chappell, 2001) and +3–5 m (eastern coast of
754 the USA; Wehmiller et al., 2004), with a -20 m mean value based on curves by Lea et al. (2002)
755 and Waelbroeck et al. (2002; Fig. 12). However, our sea level estimation for MIS 5a peak agrees
756 with that by Shackleton (2000) and data from Bahamas (Neumann and Hearty, 1996), Bermuda
757 (Hearty, 2002) and western Mediterranean. In particular, using data from phreatic overgrowths
758 on speleothems from Mallorca Island, Dorale et al. (2010) and Ginés et al. (2012) inferred
759 elevations of c. +1 m and +1.5–2.5 m for MIS 5a peak, respectively. Consistently, a MIS 5a level
760 of +1.5–2 m is estimated by geomorphological evidence and beach deposits from stable areas of
761 southern Italy, namely Sorrento peninsula and Salento (locations in Fig. 1a; Belluomini et al.,
762 2002; Iannace et al., 2003; Mastronuzzi et al., 2007). Using the Ogliastro speleothem a ~78 ka
763 age limit to MIS 5a peak and an upper limit of c. -15 m to the falling sea level at that time may
764 be inferred. Similarly the speleothem aged 90 ka indicates that during MIS 5b the sea level was
765 at least < -17 m.

766 Regarding MIS 5c peak, which based on global scale curves ranges from c. -8 m (Shackleton,
767 2000) to much below -20 m (e.g., Waelbroeck et al., 2002; Siddall, 2003; Spratt and Lisieki,
768 2016), less information is available from the Mediterranean area. The low amount of data on
769 MIS 5c somehow supports our evidence on its level less elevated than MIS 5a, and with findings
770 of MIS 5c markers essentially in areas affected by fast uplift, e.g. southern Calabria and
771 northeastern Sicily (Balescu et al., 1997; Mauz and Hussler, 2000; Bianca et al., 2011; Monaco
772 et al., 2017). An elevation of MIS 5c below the present sea level is inferred also by Bini et al.
773 (2020) for the nearby southern Cilento.
774 Assuming the 0.255±0.021 mm/y uplift rate value as constant even earlier than the Last
775 Interglacial, we infer a sea level around -37 m (-37.07±12.63 m) for MIS 6e peak. As no other
776 evidence of coeval markers is known to date in the Mediterranean, we cannot crosscheck our
777 evaluation. However, it is widely acknowledged that during MIS 6e the sea level was some tens
778 of m below the Present sea level, and our result appears consistent with some global-scale
779 estimates of MIS 6e peak at c. -30 m (Siddall et al., 2003; Shackleton, 2000), while contrasts,
780 e.g., Waelbroeck et al. (2002) and Spratt and Lisieki (2016), who place that peak below our
781 value.
782 The correlation scheme of Fig. 12 shows that the elevation of paleoshoreline T5 matches several
783 peaks. Our preferred correlation of T5 is with MIS 7 due to both field evidence discussed above
784 and the lack between the T4 and T5 of other marine terraces, which should occur if the T5 was
785 older than MIS 7. According to most global-scale curves, MIS 7 peaks were located from a few
786 to 10 m below the present mean sea level (e.g., Shackleton, 2000; Waelbroeck et al., 2002;
787 Cutler et al., 2003; Siddall et al., 2003). Correlation of T5 with MIS 7e is suggested by both our
788 correlation scheme (which would rule out a correlation with MIS 7a; Fig. 12) and evidence from

789 submerged speleothems from the Tyrrhenian Sea, which indicates that the sea level was < -18 m
790 during MIS 7c (Dutton et al., 2009). Assuming constancy in uplift, an elevation a few metres
791 below the present sea level may be inferred for MIS 7e. A comparable elevation, or below it if
792 the uplift was faster, agrees with findings of MIS 7 indicators, which in southern Italy are all
793 from tectonically raised areas (e.g., Dumas et al., 1987; Cinque and Romano, 1990; Cinque et al.,
794 1994; Amato, 2000; Bianca et al., 2011).
795 The uplift rate that we evaluated, and elevations inferred for MIS 5a and 5c, MIS 6e and MIS 7
796 peaks, all rely on an assumed MIS 5e value based on mean elevation of the Last Interglacial
797 markers in stable areas of the Mediterranean. The assumed value bears an eustatic plus a
798 component due to water load, which in the central Mediterranean caused subsidence and related
799 RSL rise during MIS 5e (e.g., Rovere et al., 2016b, Stocchi et al., 2018; Bini et al., 2020).
800 Modelling carried out to date suggests that, along the coast of central Tyrrhenian Sea, the
801 contribution of GIA is in the range of 0.75–2 m for MIS 5e markers (Stocchi et al., 2018). Even
802 assuming a 2 m value for GIA, the overestimation of the uplift rate would be in the order of 10^{-3}
803 mm/y, thus falling in uncertainty that we associated with our uplift and sea level evaluations.
804
805 **7. Concluding remarks**
806 The new morphostratigraphical and geochronological data on Basilicata - northern Calabria
807 paleoshorelines indicate that morphology of the investigated coastal stretch has been imprinted
808 by late Quaternary uplift and coeval sea level fluctuations, which have driven multiple re-
809 shaping of the coastal belt by alternating shallow marine and continental processes.
810 The estimated c. 0.25 mm/y late Quaternary uplift, of one order greater than previously
811 estimated, points to the need for both a reassessment of the age framework of the upper part of

812 the marine terrace flight in the study area and, more importantly, in depth investigations of sea
813 level markers to the south of the study area, where coral bearing deposits occur. Such
814 investigations are meaningful to the definition of the late Quaternary tectonic behaviour of a
815 coastal area struck in historical times by several moderate to strong offshore earthquakes, the
816 sources of which are still undefined.
817 The new data have allowed unravelling the presence of sea level markers related to each of the
818 eustatic peaks of MIS 5, to MIS 7 and the cooler MIS 6. In the Fiumicello and surrounding area,
819 the MIS 6e paleoshoreline has been well preserved from later erosion by burial of alluvial fan
820 deposits sourced, during younger MIS 6 substages, by frost action in the steep slopes and river
821 basins behind the coast.
822 Our findings on the vertical distribution of the dated paleoshorelines clearly demonstrate that a
823 mere sequential correlation based on assumption that the higher is the older may be strongly
824 misleading in the interpretation of flights of marine terraces. Hence, our results indicate that
825 multiple age controls are crucial to unravelling the complex interaction between uplift and sea
826 level fluctuations in tectonically active coastal areas.
827 Important implications of our data are the multiple constraints to the history of the sea level
828 fluctuations in the Tyrrhenian Sea. The net evidence of re-shaping of the coast by each of the
829 three peaks of MIS 5 and MIS 6e in a moderately uplifting area, is a clear evidence that the MIS
830 5a, 5c and 6e peaks were confined in a range, around/below the sea level, less pronounced than
831 that predicted by the most widely used sea level curves. Nonetheless, our evaluations of MIS 5a
832 and 5c peaks that according to our data are of c. + 1 m and -10 m, respectively, are consistent
833 with several findings from the western Mediterranean. The reconstructed paleo-elevations of
834 MIS 5a, 5c and MIS 6e (c. -37±12 m), besides contributing to a better definition of GIA models

for the Mediterranean, have implications on estimations of ice volume fluctuations during the late Quaternary.

Acknowledgements

We wish to acknowledge Ed Keller, Pedro Cunha and an anonymous reviewer for thoughtful and constructive criticism and Editor Martin Stokes for useful suggestions. We also thank Sylvia Riechelmann (Ruhr-Universität Bochum, Institut für Geologie, Mineralogie und Geophysik, Germany) for stable isotope analyses and the Italian Ministero dell'Ambiente della Tutela del Territorio e del Mare for making the LiDAR data available to us. This work was partially financially supported by the FFABR-E61I18001590005 Project (responsible A. Ascione).

References

Amato, A., 2000. Estimating Pleistocene tectonic uplift rates in the South-Eastern Apennines (Italy) from erosional landsurfaces and marine terraces. In Slaymaker, O. (Ed.), Geomorphology, human activity and global environmental change. Wiley, Chichester, pp. 67–87.

Antonioli, F., Ferranti, L., Lambeck, K., Kershaw, S., Verrubbi, V., Dai Pra, G., 2006. Late Pleistocene to Holocene record of changing uplift rates in southern Calabria and northeastern Sicily (southern Italy, Central Mediterranean Sea). Tectonophysics 422, 23–40. https://doi.org/10.1016/j.tecto.2006.05.003.

Antonioli, F., Lo Presti, V., Rovere, A., Ferranti, L., Anzidei, M., Furlani, S., Mastronuzzi, G., Orru, P.E., Scicchitano, G., Sannino, G., Spampinato, C.R., Pagliarulo, R., Deiana, G., de Sabata, E., Sansò, P., Vacchi, M., Vecchio, A., 2015. Tidal notches in Mediterranean Sea: a

858 comprehensive analysis. Quat. Sci. Rev. 119, 66–84.
859 https://doi.org/10.1016/j.quascirev.2015.03.016
860 Ascione, A., Ciarcia, S., Di Donato, V., Mazzoli, S., Vitale, S., 2012. The Pliocene-Quaternary
861 wedge-top basins of southern Italy: an expression of propagating lateral slab tear beneath the
862 Apennines. Basin Res. 24, 456–474. https://doi.org/10.1111/j.1365-2117.2011.00534.x
863 Ascione, A., Romano, P., 1999. Vertical movements on the eastern margin of the Tyrrhenian
864 extensional basin. New data from Mt. Bulgheria (Southern Apennines, Italy). Tectonophysics
865 315, 337–356. https://doi.org/10.1016/S0040-1951(99)00279-6
866 Balescu, S., Dumas, B., Guérémy, P., Lamothe, M., Lhenaff, R., Raffy, J. 1997.
867 Thermoluminescence dating tests of Pleistocene sediments from uplifted marine shorelines
868 along the southwest coastline of the Calabrian Peninsula (southern Italy). Palaeogeogr.
869 Palaeoclimatol. Palaeoecol. 130, 25–41.
870 Bard, E., Hamelin, B., Fairbanks, R.G., 1990. U-Th ages obtained by mass spectrometry in
871 corals from Barbados: sea level during the past 130,000 years. Nature 346, 456–458.
872 Bardají, T., Goy, J.L., Zazo, C., Hillaire-Marcel, C., Dabrio, C.J., Cabero, A., Ghaleb, B., Silva,
873 P.G., Lario, J., 2009. Sea level and climate changes during OIS 5e in the Western
874 Mediterranean. Geomorphology 104, 22–37. https://doi.org/10.1016/j.geomorph.2008.05.027
875 Belluomini, G., Caldara, M., Casini, C., Cerasoli, M., Manfra, L., Mastronuzzi, G., Palmentola,
876 G., Sanso, P., Tuccimei, P., Vesica, P.L., 2002. The age of Late Pleistocene shorelines and
877 tectonic activity of Taranto area, Southern Italy. Quat. Sci. Rev. 21, 525–547.
878 https://doi.org/S0277-3791(01)00097-X

879 Bender, M., Fairbank, R.G., Taylor, F.W., Matthews, R.K., Goddard, J.G., Broecker, W.S., 1979.
880 Uranium series dating of the Pleistocene reef tracts of Barbados, West Indies. Geol. Soc. Amer.
881 Bull. 90, 577.
882 Benjamin, J., Rovere, A., Fontana, A., Furlani, S., Vacchi, M., Inglis, R.H., Galili, E., Antonioli,
883 F., Sivan, D., Miko, S., Mourtzas, N., Felja, I., Meredith-Williams, M., Goodman-Tchernov,
884 B., Kolaiti, E., Anzidei, M., Gehrels, R., 2017. Late Quaternary sea-level changes and early
885 human societies in the central and eastern Mediterranean Basin: An interdisciplinary review.
886 Quat. Int. 449, 29–57. https://doi.org/10.1016/j.quaint.2017.06.025
887 Bianca, M., Catalano, S., De Guidi, G., Gueli, A.M., Monaco, C., Ristuccia, G.M., Stella, G.,
888 Tortorici, G., Tortorici, L., Troja, S.O., 2011. Luminescence chronology of Pleistocene marine
889 terraces of Capo Vaticano peninsula (Calabria, Southern Italy). Quat. Int. 232, 114–121.
890 https://doi.org/10.1016/j.quaint.2010.07.013
891 Bini, M., Zanchetta, G., Drysdale, R.N., Giaccio, B., Stocchi, P., Vacchi, M., Hellstrom, J.C.,
892 Couchoud, I., Monaco, L., Ratti, A., Martini, F., Sarti, L., 2020. An end to the Last Interglacial
893 highstand before 120 ka: Relative sea-level evidence from Infreschi Cave (Southern Italy).
894 Quat. Sci. Rev. 250, 106658. https://doi.org/10.1016/j.quascirev.2020.106658
895 Bish, D.L., Post, J., 1993. Quantitative mineralogical analysis using the Rietveld full pattern
896 fitting method. Am. Mineral. 78, 932–940.
897 Bloom, A.L., W.S., B., Chappell, J.M.A., Matthews, R.K., Mesolella, K.J., 1974. Quaternary sea
898 level fluctuations on a tectonic coast: new 230Th/234U dates from the Huon Peninsula, New
899 Guinea. Quat. Res. 4, 185–205.

900 Bordoni, G., Valensise, G., 1999. Deformation of the 125-ka marine terrace in Italy: tectonic
901 implications. In: Stewart, I.S., Vita-Finzi, C. (Eds.), Coastal Tectonics, Geol. Soc. London
902 Spec. Publ. 146, 71–110.
903 Buscher, J.T., Ascione, A., Valente, E., 2017. Decoding the role of tectonics, incision and
904 lithology on drainage divide migration in the Mt. Alpi region, southern Apennines, Italy.
905 Geomorphology 276, 37-50. https://doi.org/10.1016/j.geomorph.2016.10.003.
906 Caiazzo, C., Ascione, A., Cinque, A., 2006. Late Tertiary-Quaternary tectonics of the Southern
907 Apennines (Italy): New evidences from the Tyrrhenian slope. Tectonophysics 421, 23–51.
908 https://doi.org/10.1016/j.tecto.2006.04.011
909 Carobene, L., Dai Pra, G., 1990. Genesis, chronology and tectonics of the Quaternary marine
910 terraces of the Tyrrhenian coast of northern Calabria (Italy). Their correlation with climatic
911 variations. Il Quaternario 3, 75–94.
912 Carobene, L., Dai Pra, G., 1991. Middle and Upper Pleistocene sea level highstands along the
913 Tyrrhenian coast of Basilicata (Southern Italy). Il Quaternario 4, 173–202.
914 Carobene, L., Dai Pra, G., Gewelt, M., 1986. Niveaux marins du Pléistocène moyen-supérieur de
915 la côte tyrrhénienne de la Calabre (Italie méridionale) Datations $^{230}Th/^{234}U$ et tectonique
916 récente. Zeitschrift für Geomorphol. Supp.-Bd. 62, 141–158.
917 Carvalhido, R.P., Pereira, D.I., Cunha, P.P., Buylaert, J.-P., Murray, A.S., 2014. Characterization
918 and dating of coastal deposits of NW Portugal (Minho-Neiva area): A record of climate,
919 eustasy and crustal uplift during the Quaternary. Quat. Int. 328-329, 94-106. DOI:
920 10.1016/j.quaint.2014.01.025

921 Cerrone, C., Vacchi, M., Fontana, A., Rovere, A., 2021a. Last Interglacial sea level proxies in
922 the Western Mediterranean. Earth Syst. Sci. Data Discuss. [preprint],
923 https://doi.org/10.5194/essd-2021-49, in review.
924 Cerrone, C., Di Donato, V., Mazzoli, S., Robustelli, G., Soligo, M., Tuccimei, P., Ascione, A.,
925 2021b. Development and deformation of marine terraces: Constraints to the evolution of the
926 Campania Plain Quaternary coastal basin (Italy). Geomorphology 385, 107725.
927 https://doi.org/10.1016/j.geomorph.2021.107725.
928 Chappell, J., Omura, A., Esat, T., McCulloch, M., Pandolfi, J., Ota, Y., Pillans, B., 1996.
929 Reconciliation of late Quaternary sea levels derived from coral terraces at Huon Peninsula with
930 deep sea oxygen isotope records. Earth Planet. Sci. Lett. 141(1-4), 227-236.
931 Chappell, J., Shackleton, N.J., 1986. Oxygen isotopes and sea level. Nature 324, 137–140.
932 Cinque, A., Patacca, E., Scandone, P., Tozzi, M., 1993. Quaternary kinematic evolution of the
933 Southern Apennines. Relationships between surface geological features and deep lithospheric
934 structures. Ann. Geophys. 36, 249–259.
935 Cinque, A., Romano, P., 1990. Segnalazione di nuove evidenze di antiche linee di riva in
936 Penisola Sorrentina (Campania). Geogr. Fis. Dinam. Quat. 13(1), 3-36.
937 Cinque A., Romano P., Rosskopf C., Santangelo N., Santo A., 1994. Morfologie costiere e
938 depositi quaternari tra Agropoli e Ogliastro Marina (Cilento - Italia Meridionale). Il
939 Quaternario 7(1), 3-16.
940 Creveling, J.R., Mitrovica, J.X., Hay, C.C., Austermann, J., Kopp, R.E., 2015. Revisiting
941 tectonic corrections applied to Pleistocene sea-level highstands. Quat. Sci. Rev. 111, 72–80.
942 https://doi.org/https://doi.org/10.1016/j.quascirev.2015.01.003

943 Cutler, K.B., Edwards, R.L., Taylor, F.W., Cheng, H., Adkins, J., Gallup, C.D., Cutler, P.M.,
944 Burr, G.S., Bloom, A.L., 2003. Rapid sea-level fall and deep-ocean temperature change since
945 the last interglacial period. Earth Planet. Sci. Lett. 206, 253–271.
946 https://doi.org/10.1016/S0012-821X(02)01107-X
947 Damiani, A.V., 1970. Terrazzi marini e sollevamenti differenziali fra i Bacini del Lao e del
948 Corvino (Calabria settentrionale). Ital. J. Geosci. 89, 145–158.
949 Dorale, J., Onac, B.P., Fornos, J.J., Gines, J., Gines, A., Tuccimei, P., Peate, D.W., 2010. Sea-
950 level highstand 81,000 years ago in Mallorca. Science 327, 860–863.
951 https://doi.org/10.1126/science.1181725
952 Downs, R.T., Hall-Wallace, M., 2003. The American Mineralogist crystal structure database.
953 Am. Min. 88, 247–250.
954 Dumas, B., Gueremy, P., Lhenaff, J., Raffy, R., 1987. Quaternary shorelines in Southern
955 Calabria (Italy). Zeitschrift für Geomorphol. N.F. Suppl. B.d. 63, 119–132.
956 Dumas, B., Gueremy, P., Lhenaff, R., Raffy, J., 2000. Périodicités de temps long et de temps
957 court, depuis 400000 ans, dans l'étagement des terrasses marines en Calabre méridionale
958 (Italie). Géomorphologie: Relief, Processus, Environnement 1, 25–44.
959 Dumas, B., Guérémy, P., Raffy, J., 2005. Evidence for sea-level oscillations by the
960 'characteristic thickness' of marine deposits from raised terraces of Southern Calabria (Italy).
961 Quat. Sci. Rev. 24, 2120–2136. https://doi.org/10.1016/j.quascirev.2004.12.011
962 Dutton, A., Bard, E., Antonioli, F., Esat, T.M., Lambeck, K., McCulloch, M.T. 2009. Phasing
963 and amplitude of sea-level and climate change during the penultimate interglacial. Nature
964 Geosci. 2(5), 355-359. DOI:10.1038/NGEO470

965 Dutton, A., Lambeck, K., 2012. Ice volume and sea level during the Last Interglacial. Science
966 337, 216–219. https://doi.org/10.1126/science.1205749
967 Edwards, R.L., Gallup, C. D., Cheng, H., 2003. Uranium-series Dating of Marine and Lacustrine
968 Carbonates. In: Bourdon, B., Henderson, G.M., Lundstrom, C.C., Turner, S.P. (Eds.), Uranium-
969 series geochemistry, Reviews in Mineral. Geochem. 52, 363-405.
970 Esposito, C., Filocamo, F., Marciano, R., Romano, P., Santangelo, N., Scarciglia, F., Tuccimei,
971 P., 2003. Late Quaternary shorelines in southern Cilento (Mt. Bulgheria): morphostratigraphy
972 and chronology. Il Quaternario 16(1), 3–14.
973 Faccenna, C., Becker, T.W., Lucente, F.P., Jolivet, L., Rossetti, F., 2001. History of subduction
974 and back-arc extension in the Central Mediterranean. J. Geophys. Res. 145, 809–820.
975 Faccenna, C., Molin, P., Orecchio, B., Olivetti, V., Bellier, O., Funiciello, F., Minelli, L.,
976 Piromallo, C., Billi, A., 2011. Topography of the Calabria subduction zone (southern Italy):
977 Clues for the origin of Mt. Etna. Tectonics, 30, TC1003, doi:10.1029/2010TC002694.
978 Ferranti, L., Antonioli, F., Mauz, B., Amorosi, A., Dai Pra, G., Mastronuzzi, G., Monaco, C.,
979 Orrù, P., Pappalardo, M., Radtke, U., Renda, P., Romano, P., Sansò, P., Verrubbi, V., 2006.
980 Markers of the last interglacial sea-level high stand along the coast of Italy: Tectonic
981 implications. Quat. Int. 145–146, 30–54. https://doi.org/10.1016/j.quaint.2005.07.009
982 Ferranti, L., Antonioli, F., 2007. Misure del solco Tirreniano (MIS 5.5) nell'isola di Capri:
983 valutazione di attività tettonica durante il Pleistocene superiore. Il Quaternario 20(2), 125-136.
984 Ferranti, L., Monaco, C., Antonioli, F., Maschio, L., Kershaw, S., Verrubbi, V., 2007. The
985 contribution of regional uplift and coseismic slip to the vertical crustal motion in the Messina
986 Strait, southern Italy: Evidence from raised Late Holocene shorelines. J. Geophys. Res. 112,
987 B06401. https://doi.org/10.1029/2006JB004473

988 Filocamo, F., 2007. Evoluzione quaternaria del margine tirrenico dell'Appennino meridionale tra
989 il Golfo di Sapri e la foce del fiume Lao: studio stratigrafico e geomorfologico. PhD Thesis,
990 Federico II University, Napoli, Italy, 340 pp. Available at http://www.fedoa.unina.it.
991 Filocamo, F., Romano, P., Di Donato, V., Esposito, P., Mattei, M., Porreca, M., Robustelli, G.,
992 Russo Ermolli, E., 2009. Geomorphology and tectonics of uplifted coasts: New
993 chronostratigraphical constraints for the Quaternary evolution of Tyrrhenian North Calabria
994 (southern Italy). Geomorphology 105, 334–354.
995 https://doi.org/10.1016/j.geomorph.2008.10.011
996 Ford, D.C., Williams, P.W., 1989. Karst Geomorphology and Hydrology. Unwin Hyman,
997 London.
998 Gardner, T., Marshall, J., Merritts, D., Bee, B., Burgette, R., Burton, E., Cooke, J., Kehrwald, N.,
999 Protti, M., Fisher, D., Sak, P., 2001. Holocene forearc block rotation in response to seamount
1000 subduction, southeastern Peninsula de Nicoya, Costa Rica. Geology 29(2), 151-154.
1001 https://doi.org/10.1130/0091-7613(2001)029<0151:HFBRIR>2.0.CO;2
1002 Ghisetti, F., 1992. Fault parameters in the Messina Strait (southern Italy) and relations with the
1003 seismogenic source. Tectonophysics 210, 117–133. https://doi.org/10.1016/0040-
1004 1951(92)90131-O
1005 Ginés, J., Ginés, A., Fornós, J.J., Tuccimei, P., Onac, B.P., Gràcia, F., 2012. Phreatic
1006 Overgrowths on Speleothems (POS) from Mallorca, Spain: Updating forty years of research. In
1007 Ginés, A., Ginés, J., Gómez-Pujol, L., Onac, B.P., Fornós, J.J. (eds) 2012. Mallorca: A
1008 Mediterranean benchmark for Quaternary Studies. Mem. Soc. Nat. Balears 18, 111-146. ISBN
1009 978-84-7632-995-5.

1010 Gvirtzman, Z., Nur, A., 1999. The formation of Mount Etna as the consequence of slab rollback,
1011 Nature 401, 782–785.
1012 Hearty, P.J., Hollin, J.T., Neumann, A.C., O'Leary, M.J., McCulloch, M., 2007. Global sea-level
1013 fluctuations during the Last Interglaciation (MIS 5e). Quat. Sci. Rev. 26, 2090–2112.
1014 https://doi.org/10.1016/j.quascirev.2007.06.019
1015 Hearty, P.J., 2002. Revision of the late Pleistocene stratigraphy of Bermuda. Sediment. Geol.
1016 153, 1–21. https://doi.org/10.1016/S0037-0738(02)00261-0
1017 Huybers, P., Aharonson, O., 2010. Orbital tuning, eccentricity, and the frequency modulation of
1018 climatic precession. Paleoceanography 25, PA4228, doi:10.1029/2010PA001952.
1019 Imbrie, J., Hays, J., Martinson, D., McIntyre, A., Mix, A., Morley, J., Pisias, N., Prell, W.,
1020 Shackleton, N., 1984. The orbital theory of Pleistocene climate: Support from a revised
1021 chronology of the marine $\delta^{18}O$ record. In: Berger A. et al. (Eds.), Milankovitch and Climate:
1022 Understanding the response to astronomical forcing, Part 1, D. Riedel Publishing, Dordrecht,
1023 Netherlands, pp. 269-305.
1024 Iannace, A., Romano, P., Tuccimei, P., 2003. U/Th dating and geochemistry of carbonate
1025 concretions associated with upper Pleistocene fossil shorelines of the Sorrento Peninsula
1026 (Conca dei Marini, southern Italy). Il Quaternario 6(1Bis), 49–54.
1027 Iannace, A., Bonardi, G., D'Errico, M., Mazzoli, S., Perrone, V., Vitale, S., 2005. Structural
1028 setting and tectonic evolution of the Apennine Units of northern Calabria. Comptes Rendus
1029 Geosci. 337, 1541–1550. https://doi.org/10.1016/j.crte.2005.09.003
1030 Iannace, A., Vitale, S., D'Errico, M., Mazzoli, S., Di Staso, A., Macaione, E., Messina, A.,
1031 Reddy, S.M., Somma, R., Zamparelli, V., Zattin, M., Bonardi, G., 2007. The carbonate tectonic
1032 units of northern Calabria (Italy): a record of Apulian palaeomargin evolution and Miocene

convergence, continental crust subduction, and exhumation of HP-LT rocks. J. Geol. Soc. London 164, 1165–1186.

IPCC, Stocker, T.F., Qin, D., Plattner, G.-K., Tignor, M., Allen, S.K., Boschung, J., Nauels, A., Xia, Y., Bex, V., Midgley, P.M., 2013. Climate Change. The Physical Science Basis. Working Group, I Contribution to Fifth Assessment Report of the Intergovernmental Panel on Climate Change-Abstract for Decision-Makers.

Ivanovich, M., Vita-Finzi, C., Hennig, G.J., 1983. Uranium-series dating of molluscs from uplifted Holocene beaches in the Persian Gulf. Nature 302, 408–410. https://doi.org/10.1038/302408a0

Jara-Muñoz, J., Melnick, D., Pedoja, K., Strecker, M.R., 2019. TerraceM-2: A Matlab R interface for mapping and modeling marine and lacustrine terraces. Front. Earth Sci. 7:255, 1–18. https://doi.org/10.3389/feart.2019.00255

Kattsov, V.M., Källén, E., Cattle, H.P., Christensen, J., Drange, H., Hanssen-Bauer, I., Jóhannesen, T., Karol, I., Räisänen, J., Svensson, G., 2005. Future Climate Change: Modeling and Scenarios for Arctic. Arctic Climate Impact Assessment (ACIA) Overview Report, Cambridge University Press, New York, pp. 99-150.

Kaufman, A., Broecker, W., 1965. Comparison of Th230 and C14 ages for carbonate materials from lakes Lahontan and Bonneville. J. Geophys. Res. 70, 4039–4054. https://doi.org/10.1029/JZ070i016p04039

Kaufman, A., Broeker,W.S., Ku, T.L., Thurber, D.L., 1971. The status of U-series methods of mollusk dating. Geochim. Cosmochim. Acta 35, 1115–1183.

1054 Kaufman, A., Ghaleb, B.,Wehmiller, J.F., Hillaire-Marcel, C., 1996. Uranium concentration and
1055 isotope ratio profiles within Mercenaria shells: geochronological implications. Geochim.
1056 Cosmochim. Acta 60, 3735–3746.
1057 Kopp, R.E., Simons, F.J., Mitrovica, J.X., Maloof, A.C., Oppenheimer, M., 2009. Probabilistic
1058 assessment of sea level during the last interglacial stage. Nature 462, 863–868.
1059 https://doi.org/10.1038/nature08686
1060 Lajoie, K., 1986. Coastal tectonics. In: Usselman, T.M. (Ed.), Studies in Geophysics, Active
1061 Tectonics. National Academy Press, Washington DC, pp. 95–124.
1062 Lambeck, K., Chappell, J., 2001. Sea Level Change Through the Last Glacial Cycle. Science
1063 292, 679–686. https://doi.org/10.1126/science.1059549
1064 Lambeck, K., Antonioli, F., Purcell, T., Stirling, C.H., 2004. MIS 5.5 Sea level in the
1065 Mediterranean and inferences on the Global Ice Volumes during late MIS 6 and MIS 5.5. Proc.
1066 32nd Int. Geol. Congr. Florence, Italy.
1067 Larson, A. C., Von Dreele, R.B., 2004. General Structure Analysis System (GSAS), Los Alamos
1068 National Laboratory Report LAUR 86-748.
1069 Lawrence Edwards, R., Chen, J.H., Wasserburg, G.J., 1987. $^{238}U^{234}U^{230}Th^{232}Th$ systematics and
1070 the precise measurement of time over the past 500,000 years. Earth Planet. Sci. Lett. 81, 175–
1071 192. https://doi.org/10.1016/0012-821X(87)90154-3
1072 Lea, D.W., Martin, P.A., Pak, D.K., Spero, H.J., 2002. Reconstructing a 350 ky history of sea
1073 level using planktonic Mg/Ca and oxygen isotope records from a Cocos Ridge core. Quat. Sci.
1074 Rev. 21, 283–293.
1075 Lisiecki, L.E., Raymo, M.E., 2005. A Pliocene-Pleistocene stack of 57 globally distributed
1076 benthic $\delta^{18}O$ records. Paleoceanography 20, 1–17. https://doi.org/10.1029/2004PA001071

1077 Locati M., Camassi R., Rovida A., Ercolani E., Bernardini F., Castelli V., Caracciolo C.H.,
1078 Tertulliani A., Rossi A., Azzaro R., D'Amico S., Antonucci A., 2019. Database Macrosismico
1079 Italiano (DBMI15), versione 2.0. Istituto Nazionale di Geofisica e Vulcanologia (INGV).
1080 https://doi.org/10.13127/DBMI/DBMI15.3 (accessed July 2021)
1081 Ludwig, K.R., 2003. User's Manual for Isoplot 3.00: A Geochronological Toolkit for Microsoft
1082 Excel, Special publication/Berkeley Geochronology Center.
1083 Malinverno, A., Ryan, W., 1986. Extension in the Tyrrhenian sea and shortening in the
1084 Apennines as result of arc migration driven by sinking of the lithosphere. Tectonics 5, 227–245.
1085 https://doi.org/10.1029/TC005i002p00227
1086 Mastronuzzi, G., Quinif, Y., Sansò, P., Selleri, G., 2007. Middle-Late Pleistocene polycyclic
1087 evolution of a stable coastal area (southern Apulia, Italy). Geomorphology 86, 393–408.
1088 https://doi.org/10.1016/j.geomorph.2006.09.014
1089 Mauz, B., Hassler, U., 2000. Luminescence chronology of Late Pleistocene raised beaches in
1090 southern Italy: new data of relative sea-level changes. Mar. Geol. 170, 187–203.
1091 Mazzoli, S., Ascione, A., Buscher, J.T., Pignalosa, A., Valente, E., Zattin, M., 2014. Low-angle
1092 normal faulting and focused exhumation associated with late Pliocene change in tectonic style
1093 in the southern Apennines (Italy). Tectonics 33, 1802–1818. doi:10.1002/2014TC003608.
1094 Monaco, C., Barreca, G., Di Stefano, A., 2017. Quaternary marine terraces and fault activity in
1095 the northern mainland sectors of the Messina Strait (southern Italy). Ital. J. Geosci. 136, 337–
1096 346. https://doi.org/10.3301/IJG.2016.10
1097 Morel, D. L., Morell, K. D., Keller, E.A., Rittenour, T.M., 2021. Quaternary chronology and
1098 rock uplift recorded by marine terraces, Gaviota coast, Santa Barbara County, California, USA.
1099 Geol. Soc. Am. Bull., in press. doi: https://doi.org/10.1130/B35609.1

Miyauchi, T., Dai Pra, G., Sylos Labini, S., 1994. Geochronology of Pleistocene marine terraces and regional tectonics in the Tyrrhenian coast of South Calabria, Italy. Il Quaternario 7, 17–34.

Mörner, N., 1982. Sea level curves. In: Beaches and Coastal Geology. Encyclopedia of Earth Sciences Series. Springer, New York, NY. https://doi.org/https://doi.org/10.1007/0-387-30843-1_399

Moussat, E., Rehault, J.P., Fabbri, A., 1986. Rifting et èvolution tectono-sèdimentaire du Bassin Tyrrhènien au cours du Neogene et du Quaternaire. Giorn. di Geol. Serie 3 48, 1/2, 41–62.

Neumann, A.C., Hearty, P.J., 1996. Rapid sea-level changes at the close of the last interglacial (substage 5e) recorded in Bahamian Island geology. Geology 24, 775–778.

Patacca, E., Sartori, R., Scandone, P., 1990. Tyrrhenian basin and Apenninic Arcs: kinematic relations since Late Tortonian times. Mem. Soc. Geol. It 45, 425–451. https://doi.org/10.1007/978-94-011-2016-6_7.

Patacca, E., Scandone, P., 2001. Late thrust propagation and sedimentary response in the thrust-belt—foredeep system of the Southern Apennines (Pliocene-Pleistocene). In: Vai, G.B., Martini, I.P. (Eds.), Anatomy of an Orogen: the Apennines and Adjacent Mediterranean Basins. Kluwer Academic Publishers, London, pp. 401–440. https://doi.org/10.1007/978-94-015-9829-3_23.

Pedoja, K., Husson, L., Johnson, M.E., Melnick, D., Witt, C., Pochat, S., Nexer, M., Delcaillau, B., Pinegina, T., Poprawski, Y., Authemayouj, C., Elliot, M., Regard, V., Garestier, F., 2014. Coastal staircase sequences reflecting sea-level oscillations and tectonic uplift during the Quaternary and Neogene. Earth-Sci. Rev. 132, 13-38.

1121 Pirazzoli, P.A., Radtke, U., Hantoro, W.S., Jounnic, C., Hoang, C.T., Causse, C., Borell Best,
1122 M., 1993. A one million-year-long sequence of marine terraces on Sumba Island, Indonesia.
1123 Mar. Geol. 109, 221–236.
1124 Pirazzoli, P.A., 1996. Sea-level changes: The last 20,000 years. John Wiley & Sons, Chichester,
1125 210 p.
1126 Piromallo, C., Morelli A., 2003. P wave tomography of the mantle under the Alpine-
1127 Mediterranean area. J . Geophys . Res. 108(B2), 2065. doi:10.1029/2002JB001757.
1128 Polyak, V.J., Onac, B.P., Fornòs, J.J., Hay, C., Asmerom, Y., Dorale, J.A., Ginés, J., Tuccimei,
1129 P., Ginés, A., 2018. A highly resolved record of relative sea level in the western Mediterranean
1130 Sea during the last interglacial period. Nat. Geosci. 11, 860-864.
1131 Ramos, A., Cunha, P.P., Cunha, L., Gomes, A., Lopes, F.C., Buylaert, J.-P., Murray, A.S., 2012.
1132 The River Mondego terraces at the Figueira da Foz coastal area (western central Portugal):
1133 geomorphological and sedimentological characterization of a terrace staircase affected by
1134 differential uplift and glacio-eustasy. Geomorphology 165-166, 107-123. DOI:
1135 10.1016/j.geomorph.2012.03.037.
1136 Rehault, J.P., Moussat, E., Fabbri, A., 1987. Structural evolution of the Tyrrhenian back-arc
1137 basin. Mar. Geol. 74, 123–150.
1138 Roberts, G.P., Houghton, S.L., Underwood, C., Papanikolaou, I., Cowie, P.A., van Calsteren, P.,
1139 Wigley, T., Cooper, F.J., McArthur, J.M., 2009. Localization of Quaternary slip rates in an
1140 active rift in 10^5 years: An example from central Greece constrained by ^{234}U- ^{230}Th coral dates
1141 from uplifted paleoshorelines. J. Geophys. Res. 114, B10406.
1142 https://doi.org/10.1029/2008JB005818

1143 Robertson, J., Meschis, M., Roberts, G.P., Ganas, A., Gheorghiu, D.M., 2019. Temporally
1144 constant Quaternary uplift rates and their relationship with extensional upper- plate faults in
1145 south Crete (Greece), constrained with ^{36}Cl cosmogenic exposure dating. Tectonics 38(4),
1146 1189-1222.
1147 Robustelli, G., 2019. Geomorphic constraints on uplift history in the Aspromonte Massif,
1148 southern Italy. Geomorphology 327, 319–337. https://doi.org/10.1016/j.geomorph.2018.11.011
1149 Rohling, E.J., Hibbert, F.D., Grant, K.M., Galaasen, E.V., Irvali, N., Kleiven, H.F., Marino, G.,
1150 Ninnemann, U., Roberts, A.P., Rosenthal, Y., 2019. Asynchronous Antarctic and Greenland
1151 ice-volume contributions to the last interglacial sealevel highstand. Nat. Commun. 10, 5040.
1152 https://doi.org/10.1038/s41467-019-12874-3.
1153 Rovere, A., Raymo, M.E., Vacchi, M., Lorscheid, T., Stocchi, P., Gómez-Pujol, L., Harris, D.L.,
1154 Casella, E., Leary, M.J.O., Hearty, P.J., 2016a. The analysis of Last Interglacial (MIS 5e)
1155 relative sea-level indicators: Reconstructing sea level in a warmer world. Earth Sci. Rev. 159,
1156 404–427. https://doi.org/10.1016/j.earscirev.2016.06.006
1157 Rovere, A., Stocchi, Paolo, Vacchi, M., 2016b. Eustatic and Relative Sea Level Changes. Curr.
1158 Clim. Chang. Reports 221–231. https://doi.org/10.1007/s40641-016-0045-7
1159 Rovida A., Locati M., Camassi R., Lolli B., Gasperini P., Antonucci A. (eds), 2021. Italian
1160 Parametric Earthquake Catalogue (CPTI15), version 3.0. Istituto Nazionale di Geofisica e
1161 Vulcanologia (INGV). https://doi.org/10.13127/CPTI/CPTI15.2 (accessed July 2021)
1162 Royden, L.H., 1993. Evolution of retreating subduction boundaries formed during continental
1163 collision, Tectonics 12, 629–638.
1164 Scarciglia, F., Pulice, I., 2006. Soil chronosequences on Quaternary marine terraces along the
1165 northwestern coast of Calabria (Southern Italy). Quat. Int. 156–157, 133–155.

Shackleton, N.J., 2000. The 100,000 year ice age cycle identified and found to lag temperature, carbon dioxide and orbital eccentricity. Science 289, 1897–1902.

Shackleton, N.J., Berger, A., Peltier, W.R., 1990. An alternative astronomical calibration of the lower Pleistocene timescale based on ODP site 677, Trans. R. Soc. Edinburgh 81, 251-261.

Shackleton, N.J., Chapman, M., Sánchez-Goni, M.F., Pailler, D., Lancelot, Y., 2002. The classic marine isotope substage 5e. Quat. Res. 58, 14–16. https://doi.org/10.1006/qres.2001.2312

Siddall, M., Rohling, E.J., Almogi-Labin, A., Hemleben, C., Meischner, D., Schmelzer, I., Smeed, D., 2003. Sea-level fluctuations during the last glacial cycle. Nature 423, 853–858. https://doi.org/10.1038/nature01690

Siddall, M., Chappell, J., Potter, E.K., 2007. Eustatic sea level during past interglacials. In: Sirocko, F., Claussen, M., Sánchez Goñi, M.F., Litt, T. (Eds), The Climate of Past Interglacials, Developments in Quaternary Sciences 7, Elsevier, pp. 75-92. https://doi.org/10.1016/S1571-0866(07)80032-7

Sivan, D., Sisma-Ventura, G., Greenbaum, N., Bialik, O.M., Williams, F.H., Tamisiea, M.E., Rohling, E.J., Frumkin, A., Avnaim-Katav, S., Shtienberg, G., Stein, M., 2016. Eastern Mediterranean sea levels through the last interglacial from a coastal-marine sequence in northern Israel. Quat. Sci. Rev. 145, 204–225. https://doi.org/10.1016/j.quascirev.2016.06.001

Spratt, R.M., Lisiecki, L.E., 2016. A Late Pleistocene sea level stack. Clim. Past 12, 1079–1092. https://doi.org/10.5194/cp-12-1079-2016

Stirling, C.H.Ł., Esat, T.M., Lambeck, K., Mcculloch, M.T., 1998. Timing and duration of the Last Interglacial: evidence for a restricted interval of widespread coral reef growth. Earth Planet. Sci. Lett. 160, 745–762.

Stocchi, P., Vacchi, M., Lorscheid, T., de Boer, B., Simms, A.R., van de Wal, R.S.W., Vermeersen, B.L.A., Pappalardo, M., Rovere, A., 2018. MIS 5e relative sea-level changes in the Mediterranean Sea: Contribution of isostatic disequilibrium. Quat. Sci. Rev. 185, 122–134. https://doi.org/10.1016/j.quascirev.2018.01.004

Toby, B.H., 2001. EXPGUI, a graphical user interface for GSAS. J. Appl. Crystallogr. 34, 210–213.

Torres, T., Ortiz, J.E., Arribas, I., 2013. Variations in racemization/epimerization ratios and amino acid content of Glycymeris shells in raised marine deposits in the Mediterranean. Quat. Geochronol. 16, 35–49. https://doi.org/10.1016/j.quageo.2012.11.002

Tortorici, G., Bianca, M., de Guidi, G., Monaco, C., Tortorici, L., 2003. Fault activity and marine terracing in the Capo Vaticano area (southern Calabria) during the Middle-Late Quaternary. Quat. Int. 101–102, 269–278. https://doi.org/10.1016/S1040-6182(02)00107-6

Tuccimei, P., Gines, J., Gracia, F., Fornos, J.J., Taddeucci, A., 2006. Last interglacial sea level changes in Mallorca island (Western Mediterranean). High precision U-series data from phreatic overgrowths on speleothems. Zeitschrift für Geomorphol. 50, 1–21.

Turney, C.S.M., Jones, R.T., 2010. Does the Agulhas Current amplify global temperatures during super-interglacials? J. Quat. Sci. 25, 839–843. https://doi.org/10.1002/jqs.1423

Van De Plassche, O., 1986. Introduction. In: Van De Plassche O. (Ed.), Sea-level Research a manual for the collection and evaluation of data, Springer Netherlands, Dordrecht, pp. 1–23. https://doi.org/10.1007/978-94-009-4215-8_1.

Vesica, P.L., Tuccimei, P., Turi, B., Fornós, J.J., Ginés, A., Ginés, J., 2000. Late Pleistocene Paleoclimates and sea-level change in the Mediterranean as inferred from stable isotope and U-

series studies of overgrowths on speleothems, Mallorca, Spain. Quat. Sci. Rev. 19, 865–879. https://doi.org/10.1016/S0277-3791(99)00026-8

Yokoyama, Y., Lambeck, K., De Deckker, P.P.J., Fifield, L.K., 2000. Timing of the last glacial maximum from observed sea-level minima. Nature 406, 713–716.

Waelbroeck, C., Labeyrie, L., Michel, E., Duplessy, J.C., McManus, J.F., Lambeck, K., Balbon, E., Labracherie, M., 2002. Sea-level and deep water temperature changes derived from benthic foraminifera isotopic records. Quat. Sci. Rev. 21, 295–305. https://doi.org/10.1016/S0277-3791(01)00101-9.

Wehmiller, J.F., Simmons, K.R., Cheng, H., Edwards, R.L., Martin-mcnaughton, J., York, L.L., Krantz, D.E., Shen, C., 2004. Uranium-series coral ages from the US Atlantic Coastal Plain – the '80 ka problem' revisited. Quat. Int. 120, 3–14. https://doi.org/10.1016/j.quaint.2004.01.002

Westaway, R., 1993. Quaternary uplift of southern Italy. J. Geophys. Res. 98, 21741–21772. https://doi.org/10.1029/93JB01566.

Wortel, M.J.R., Spakman W., 2000. Subduction and slab detachment in the Mediterranean-Carpathian region, Science 290, 1910–1917.

Zazo, C., Goy Goy, J.L., Hillaire-Marcel, C., Gillot, P.-Y., Soler, V., González, J.-Á., Dabrio, C.J., Ghaleb, B., 2002. Raised marine sequences of Lanzarote and Fuerteventura revisited- a reappraisal of relative sea-level changes and vertical movements in the eastern Canary Islands during the Quaternary. Quat. Sci. Rev. 21(18-19), 2019-2046.

CAPTIONS TO FIGURES

Figure 1. a: Simplified tectonic sketch of the Tyrrhenian Sea basin and southern Apennines mountain belt (redrawn and modified after Moussat et al., 1986), with indication of the study area (box). b: Geological sketch of the study area (redrawn and modified after Iannace et al., 2007), with indication of the study sites.

Figure 2. Geomorphological map for the northern Calabria - Basilicata coastal sector. Insets a to e show magnifications of key areas located in the main map (dashed boxes).

Figure 3. Marine terrace T1 at Fiumicello (a to d) and Ogliastro (e and f). a: View of marine terrace T1 covered by UU alluvial fan deposit. b: The T1 calcarenite, with a *Cladocora caespitosa* globular colony (sample FMC01; location in a). c: Laminated flowstone (sample FMC07; location in a) inset in the T1 calcarenites. d and e: Contact surface, marked by a reddish paleosol, between the T1 and UU deposit in the sites of Fiumicello (diagram d) and Ogliastro (diagram e). f: T1 calcarenites filling a N-S oriented open fissure formed in the OG marine conglomerates.

Figure 4. a: T1 and T2 marine terraces in the Marina di Maratea bay (northern side). b: T2 marine succession patched onto the T1 abrasion platform and paleo-sea cliff. c: The T1 abrasion platform, with well exposed the inner edge. d: The T1 paleo-sea cliff, densely potholed by lithophaga and patched by the T2 conglomerate and calcarenites. e: Close-up view of the T2 calcarenites filling lithophaga holes in the T1 paleo-sea cliff.

Figure 5. a: Paleoshoreline T2 in the southern side of the Marina di Maratea bay and Punta Iudia (in the background), with locations of photos in diagrams b and c; note the outer rim of an abrasion platform correlated with marine terrace T4. b: T2 calcarenites erosively covered by marine arenites in the Punta Iudia site. c: T2 abrasion platform boreholed by lithophaga and partly covered by T2 calcarenites, covered by slope breccia; the calcarenites and breccia are erosively covered by arenites that mark a post-T2 RSL rise. d and e: Morphostratigraphic sketches (vertical exaggeration, horizontal scale is approximate) of the outcrops in the northern (diagram d) and southern (diagram e) sides of the Marina di Maratea bay.

Figure 6. Scalea Site, with (a) the flight of marine terraces at +60 m (T5), +35–40 m (T4) and +16 m (T2). Photos in b to e show details of marine terrace T2. b: Calcarenite bearing *C. caespitosa* growth form (sample SLC). c: Calcarenites with pit holes coated by speleothems and covered by colluvium. d: Abrasion surface with remnants of calcarenites (light grey), potholed by lithophaga. e: Calcarenites affected by m-size crevices coated by speleothems (sample SLC05) and filled with slope breccia.

Figure 7. a: Marine terrace T3 in the Grotta del Prete site, with indication of the abrasion platform, which rises from +15 m (outer edge) to 22 m (inner edge) and is covered by marine and colluvial deposits; note in the background the wide marine terrace T4 in the Torre Fiuzzi site. b: *C. caespitosa* colony (sample GRP2) included in the T3 calcarenites. c: The T3 succession, made up of conglomerates passing upwards to calcarenites, overlain by an arenite body, marked on top by a reddish paleosol.

Figure 8. a: The sea cliff behind the Castrocucco beach, with the remnants of a tidal notch at c. 35–40 m and lithophaga holes with upper limit at +20 m. Diagrams b to d show outcrops located c. 20 m a.s.l. at the southeastern edge of the Castrocucco headland. b: Neptunian dyke coated by a flowstone that is patched by calcarenites. c and d: Speleothem (sample CSC08) inset in the carbonate bedrock, potholed by densely distributed lithophaga holes and patched by marine arenites, which fill also the lithophaga holes.

Figure 9. View of Torre Fiuzzi site, with indication of marine terrace T4 and a higher marine terrace sculpted 140 m a.s.l. on the Dino Island and mainland.

Figure 10. a: Southern wall of the Madonna della Grotta cave, with evidence of the +55–60 m paleoshoreline coated by a speleothem (sample MDN01); arrow indicates the top of the marine conglomerates. b: Marine conglomerates patched on the carbonate bedrock, which is potholed by lithophaga.

Figure 11. Relative sea level curve reconstructed for the investigated sector of the southern Tyrrhenian margin. Dated paleoshorelines are indicated by circles; bars indicate paleoshoreline elevation range and uncertainty, or 2σ, of coral age. Triangles indicate dated speleothems, with age error bars; triangles are coloured according to colours of paleoshorelines that are predated, or postdated, by the each speleothem.

Figure 12. Correlation scheme for dated paleoshorelines in the investigated Tyrrhenian margin sector vs. late Quaternary sea-level peaks. The sea level curve (with confidence interval) used for reference is redrawn from Waelbroeck et al. (2002). The correlation is based on a constant 0.25

1301 mm/y uplift rate (black lines) assuming a +6 m value for MIS 5e. Dots, with error bars, mark sea
1302 level values calculated for MIS 5a, 5c and 6e; bars with arrows indicate upper limits to paleo-sea
1303 level at c. 90 ka and 78 ka.

Table 1: Results of XRD quantitative analyses (wt.%).

Sample ID	Sample type	Aragonite	Calcite	Dolomite	Quartz	Gypsum
TFZ2W	Corals	98.0	0.8			1.2
SLC	Corals	97.6	1.9	0.5		
FMCO7	Corals	97.5	2.4	0.1		
GRP2	Corals	96.9	3.1			
TFZ2	Corals	92.6	6.7		0.7	
MMRR11w	Corals	87.3	12.2		0.5	
GRP1	Corals	78.8	17.4	2.8	1.0	
FMCO8w	Corals	77.8	22.2			
FMCO8s	Corals	75.9	24.1			
MMR11s	Corals	74.1	25.4		0.5	
MMR10w	Corals	68.8	29.1			2.1
MMR10s	Corals	62.5	35.7			1.8
TFZ1	Corals	59.5	38.0	0.8	1.7	
PDR	Corals	59.0	32.5	8.5		
OLG3	Corals	1.2	98.8			
TRR1	Speleothems		100.0			

Note: the refining procedure accuracy was based on the agreement indices listed in the Table S1. The error is in the range of ± 0.5%.

Table 2 Uranium contents (mg/g), acvity ratios, and $^{230}Th/^{234}U$ ages of the analysed corals and calcite concretions (1σ). The analysed corals are *Cladocora Caespitosa* specimens with a calcite content < 3%

Sample ID	Site	Lat (°)	Long (°)	Sample type	^{238}U [mg/g]	1σ	$^{234}U/^{238}U$	1σ	$^{230}Th/^{234}U_{meas}$	1σ	$^{230}Th/^{232}Th$	1σ	$^{230}Th/^{234}U_{calc}$	1σ	Age (ka)	1σ	$^{234}U/^{238}U_{init}$	1σ
GRP2	Grotta del Prete	39.859910	15.791797	coral	2.468	± 0.062	1.150	± 0.025	0.544	± 0.016	131.844	± 12.509			83.8	± 3.6	1.190	± 0.032
SLC	Scalea	39.819173	15.783385	coral	2.066	± 0.041	1.254	± 0.024	0.608	± 0.016	146.208	± 14.051			98.0	± 4.0	1.335	± 0.032
FMC01	Fiumicello	39.998549	15.698754	coral	1.806	± 0.045	1.095	± 0.021	0.785	± 0.040	124.200	± 13.136	-	-	161	± 18	1.150	± 0.033
TFZ2W	Torre Fiuzzi	39.871695	15.786390	coral	2.287	± 0.046	1.052	± 0.018	0.673	± 0.021	87.949	± 12.641	-	-	120	±7	1.073	± 0.025
PDA2	Punta Iudia	39.954596	15.735311	speleothem	1.038	± 0.034	1.193	± 0.013	0.476	± 0.022	8.096	± 0.301	-	-	64	± 6	1.231	± 0.016
OGL2	Ogliastro	39.999880	15.690515	speleothem	0.215	± 0.005	1.009	± 0.019	0.510	± 0.015	109.354	± 14.221	-	-	78	± 3	1.011	± 0.024
MMR12	Marina di Maratea	39.958416	15.734494	speleothem	0.485	± 0.016	1.058	± 0.021	0.525	± 0.019	3.324	± 0.059	0.461	± 0.029	67	± 6	1.070	± 0.025
FMC07	Fiumicello	39.998538	15.698920	speleothem	0.598	± 0.012	1.046	± 0.011	0.532	± 0.020	60.019	± 7.583	0.528	± 0.071	81	± 5	1.082	± 0.014
MDN01	Madonna della Grotta	39.896664	15.784890	speleothem	1.067	± 0.047	0.979	± 0.018	0.814	± 0.031	1.955	± 0.061	0.749	± 0.058	152	33/-26	0.968	± 0.028
SLC05	Scalea	39.819138	15.783407	speleothem	0.539	± 0.017	1.075	± 0.018	0.634	± 0.028	6.283	± 0.245	0.602	± 0.046	99	± 12	1.099	± 0.024
PNT3	Pantano	39.897712	15.784326	speleothem	1.333	± 0.037	1.009	± 0.011	0.395	± 0.015	113.780	± 12.502			54.8	± 2.7	1.011	± 0.013
CSC8	Castrocucco	39.932927	15.746692	speleothem	0.345	± 0.006	1.018	± 0.013	0.765	± 0.022	12.745	± 0.507	0.753	± 0.026	151.0	± 11	1.028	± 0.020
MMR2	Marina di Maratea	39.958403	15.734543	speleothem	0.385	± 0.012	1.079	± 0.023	0.584	± 0.022	13.800	± 0.609	0.568	± 0.041	90.0	± 10	1.102	± 0.030
TRR1	Torre Dino	39.836211	15.769875	speleothem	10.363	± 0.452	0.980	± 0.007	0.513	± 0.034	2.288.467	± 321.587			78.8	± 7.7	0.975	± 0.008

Table 3 Correlation of dated deposits with late Quaternary Marine Isotope Stages

Sample ID	Dated deposit	MIS 3	MIS 4 and MIS 5.1 – MIS 4 transition	MIS 5					MIS 6	
				5a	5b	5c	5d	5e	6a ÷ 6f	6e
PNT3	speleothem	54.7±2.7 ka								
PDA2	speleothem		64.0±6.0 ka							
MMR12	speleothem		67.0±6.0 ka							
OGL2	speleothem		78.0±3.0 ka							
TRR1	speleothem		78.8±7.7 ka	←	78.8±7.7 ka					
FMC07	speleothem		82.0±5.0 ka	←	82.0±5.0 ka					
GRP2	coral			83.8±3.6 ka						
MMR2	speleothem				90.0±10.0 ka					
SLC05	speleothem				99.0±12.0 ka					
SLC	coral					98.0±4.0 ka				
TFZ2W	coral							120.0±7.0 ka		
CSC8	speleothem								151.0±11.0 ka	
MDN01	speleothem								152.0+33/-26 ka	
FMC01	coral									161.0±18.0 ka

Table 4 Age model for the raised paleoshorelines and correlation with Marine Isotope Stages

Paleoshoreline label	Paleoshoreline elevation (m)	Coral Th/U age (ky)	Calcite concretion Th/U age (ky)	Marine Isotope Stage
T5	57.5 ± 2.5		> 152.0 +33/-26	MIS 7
T1	5 +1/-0	161.0 ± 18.0	> 78.0 ± 3.0; > 82.0 ± 5.0	MIS 6e
T4	37.5 ± 2.5	120.0 ± 7.0	< 151.0 ± 11.0; >78.8±7.7	MIS 5e
T2	16 ± 1	98.0 ± 4.0	> 64.0 ± 6.0; > 67.0 ± 6.0; > 90.0±10.0; < 99.0 ± 12.0	MIS 5c
T3	22 ± 1	83.8 ± 3.6	> 54.7±2.7; > 67.0 ± 6.0; < 151.0 ± 11.0	MIS 5a

Figure 1 (Color)

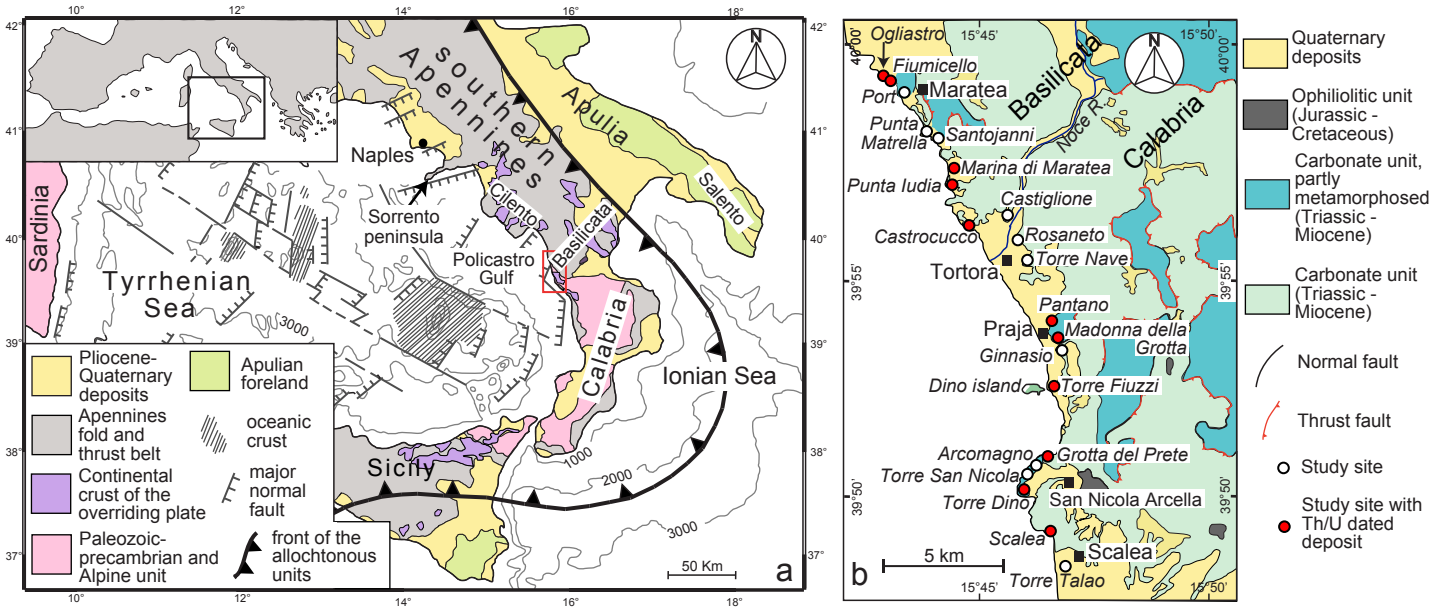

Figure 2 (Color) Click here to access/download;Figure (Color);Fig_02.tif

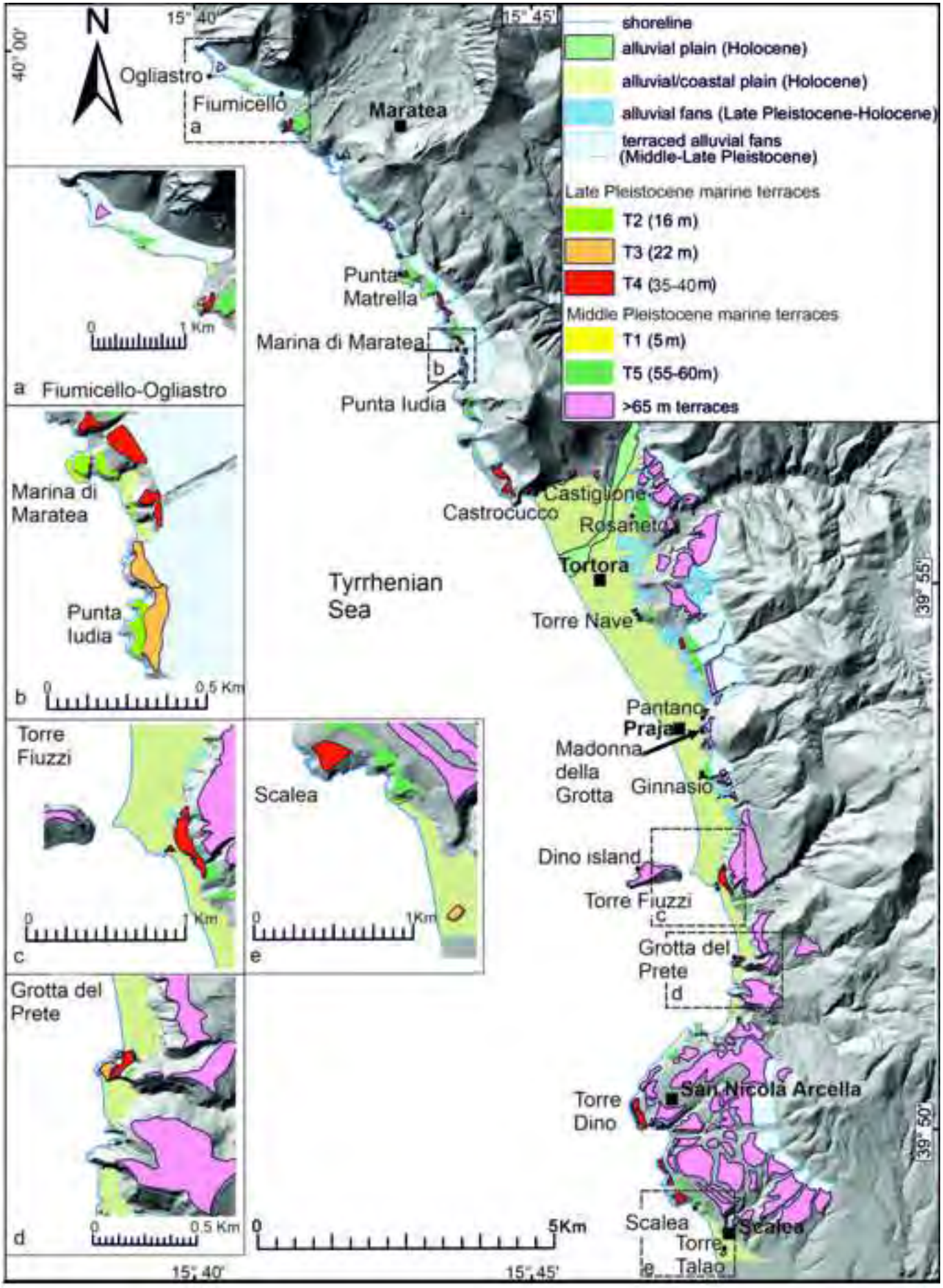

Figure 3 (Color)

Click here to access/download;Figure (Color);Fig_03.tif

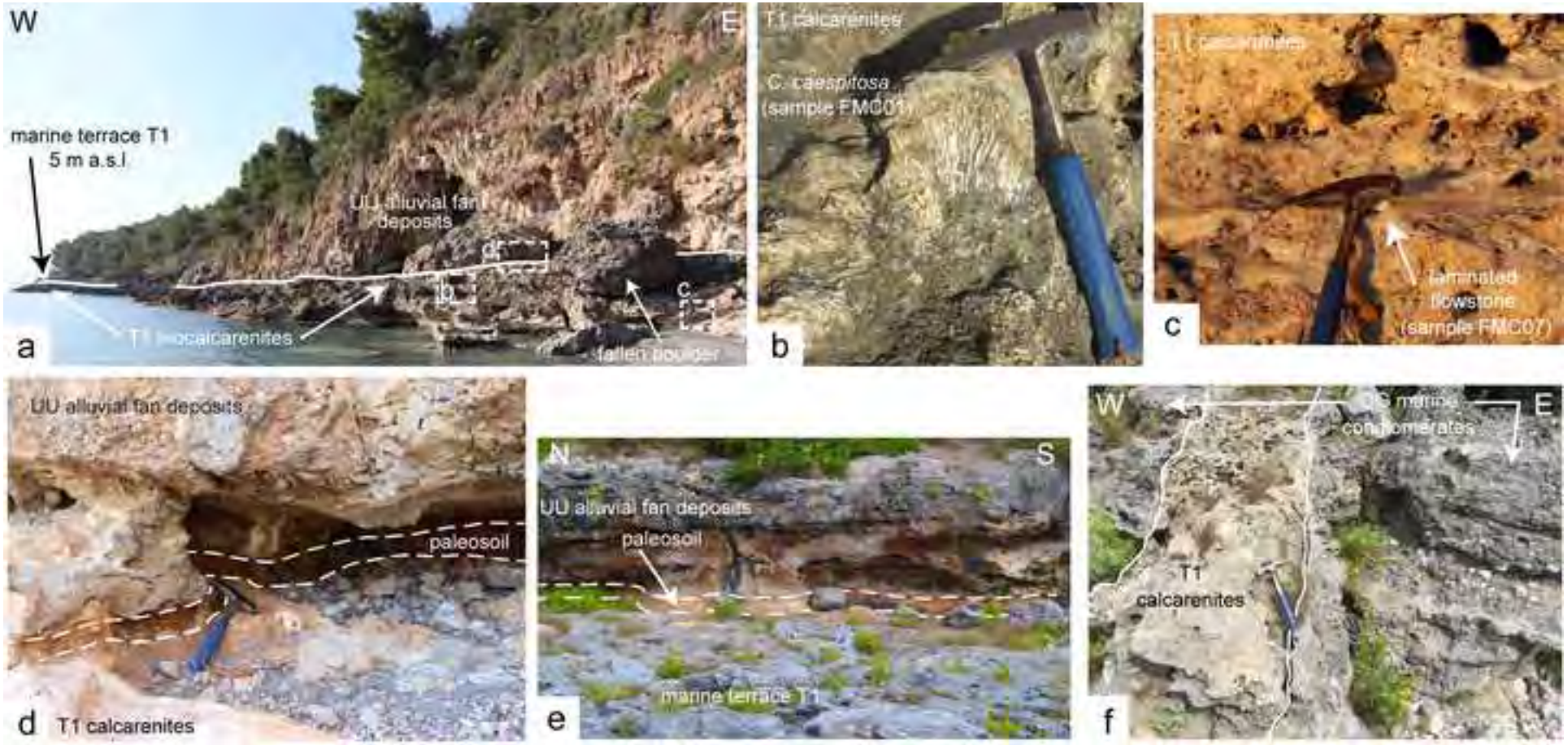

Figure 4 (Color)

Click here to access/download;Figure (Color);Fig_04.tif

Figure 5 (Color)

Click here to access/download;Figure (Color);Fig_05.tif

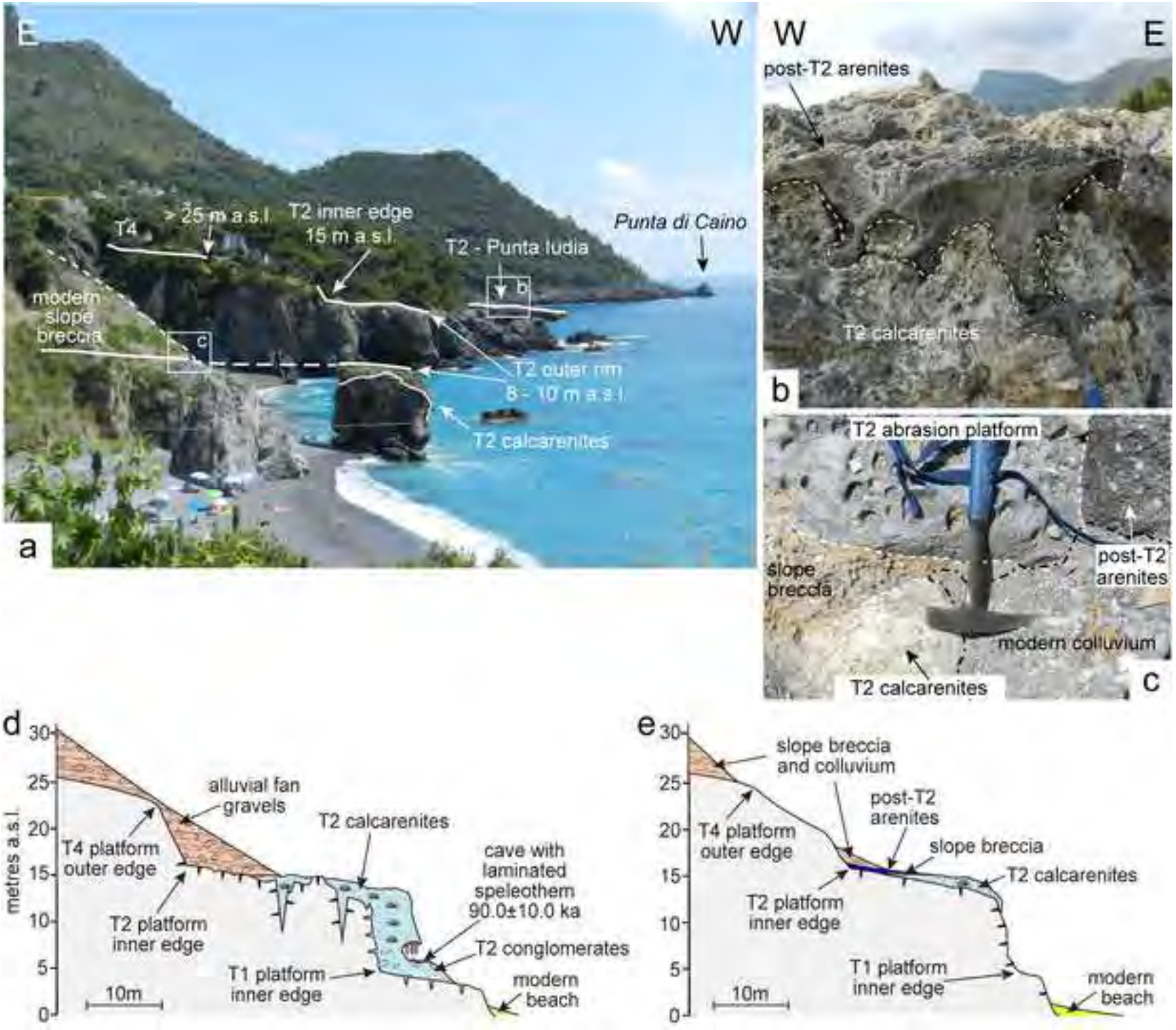

Figure 6 (Color)

Click here to access/download;Figure (Color);Fig_06.tif

Figure 7 (Color)

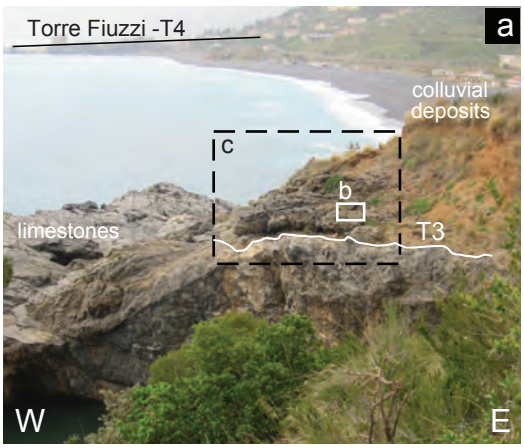

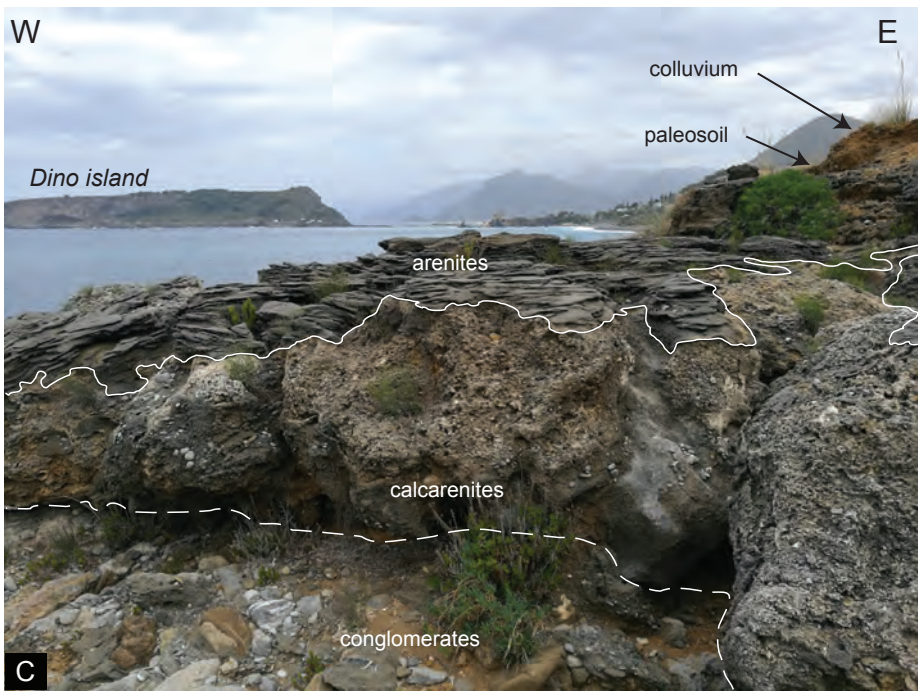

Figure 8 (Color)

Click here to access/download;Figure (Color);Fig_08.tif

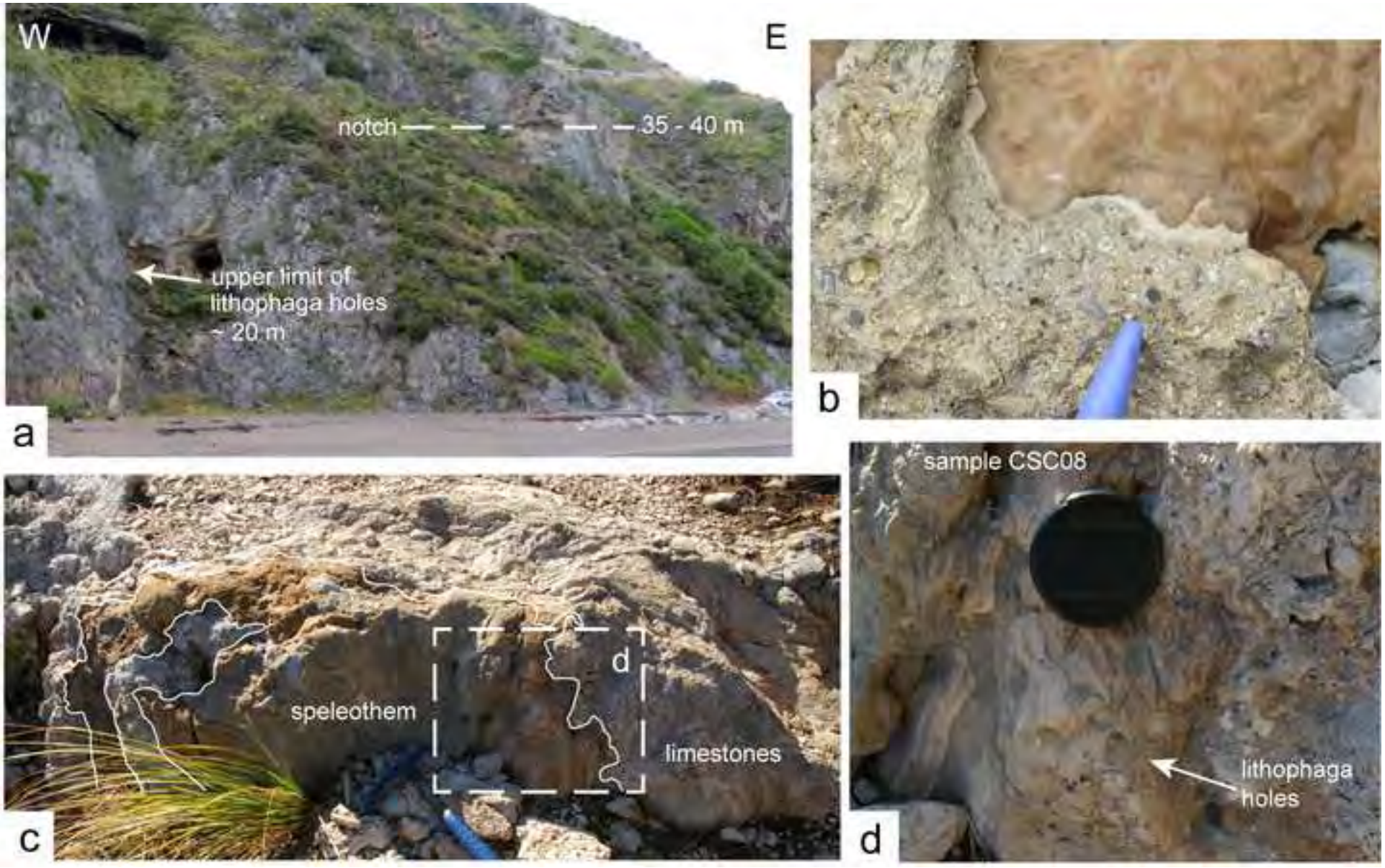

Figure 9 (Color)

Click here to access/download;Figure (Color);Fig_09.jpg

Figure 10 (Color)

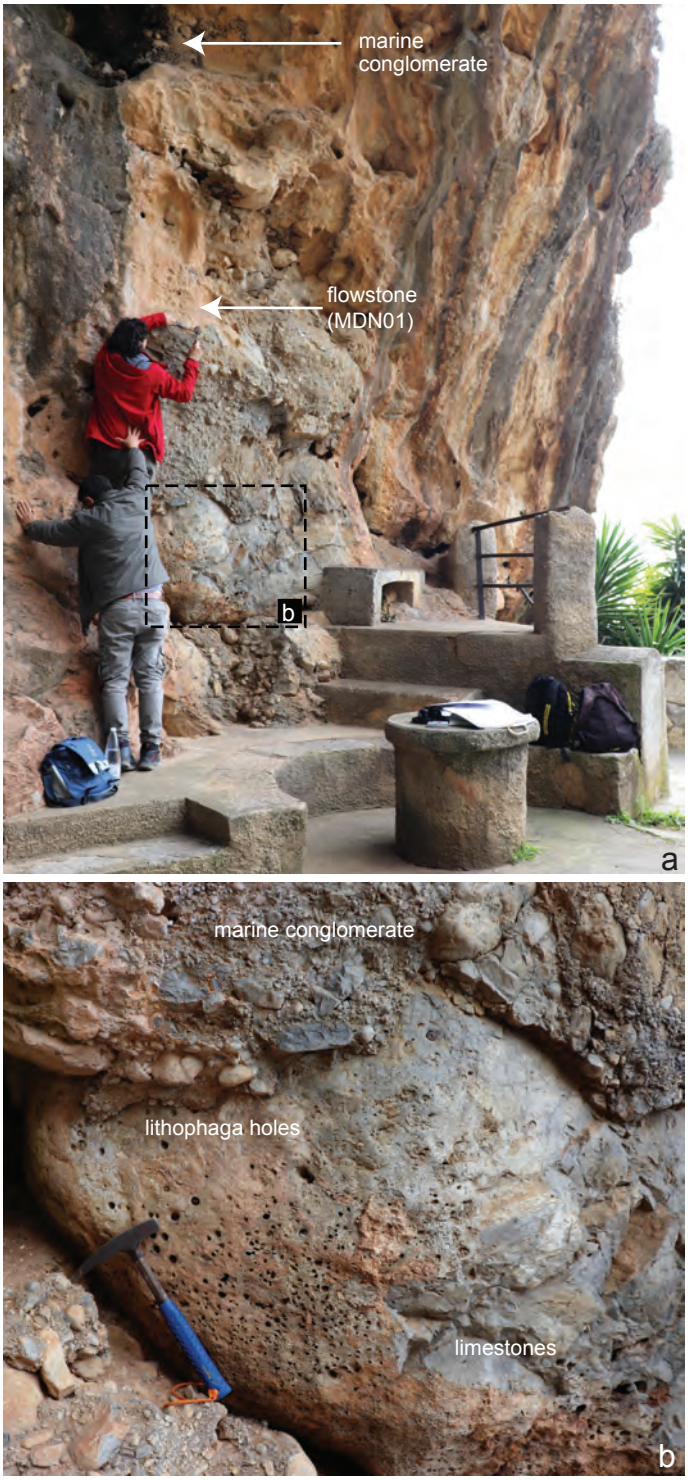

Figure 11 (Color)

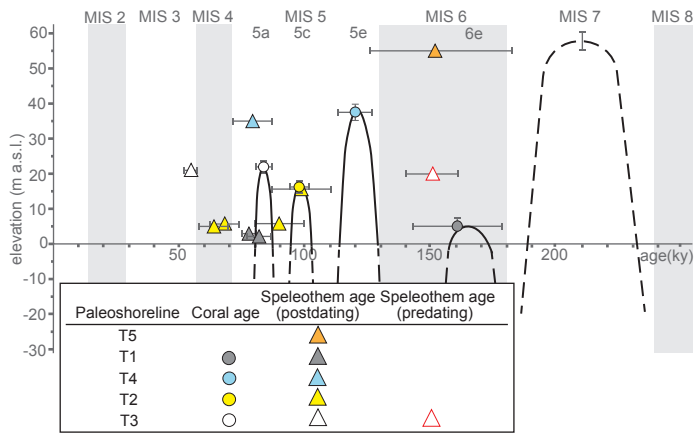

Figure 12 (Color)

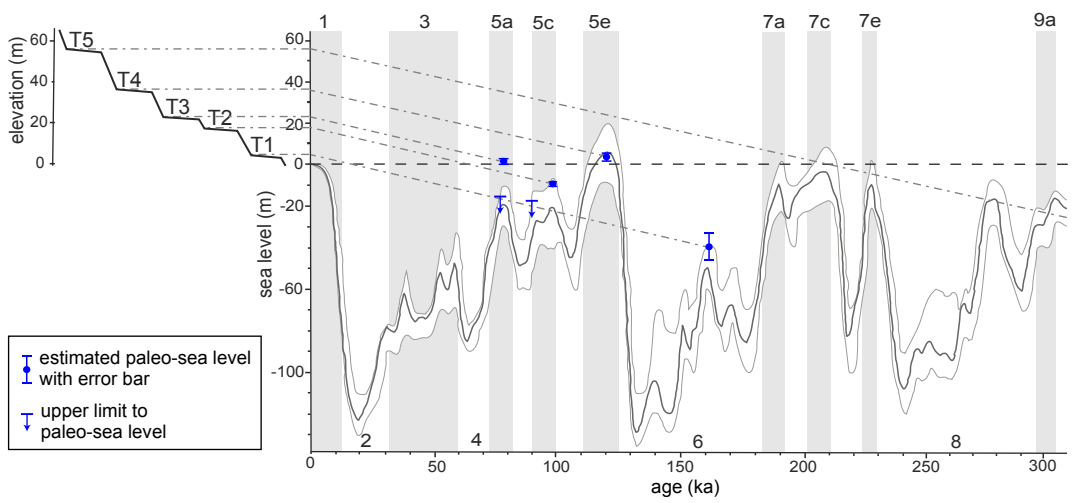

Declaration of interests

☒ The authors declare that they have no known competing financial interests or personal relationships that could have appeared to influence the work reported in this paper.

☐The authors declare the following financial interests/personal relationships which may be considered as potential competing interests:
